4-1-1969

Transverse curvature effects on turbulent boundary layers.

M. C. Joseph
University of Windsor

TRANSVERSE CURVATURE EFFECTS ON TURBULENT BOUNDARY LAYERS

A Thesis
submitted to the Faculty of Graduate Studies
in partial fulfilment of the requirements
for the degree of

Master of Applied Science
in the Department of Mechanical Engineering
University of Windsor

by

M.C.Joseph,B.E.,
Windsor, Ontario,
April, 1969.

ABD 4843

APPROVED BY: L. Li Duan.

T. H. McDonald

275366

ACKNOWLEDGEMENTS

The author wishes to express his sincere thanks to Prof. K.Sridhar and Prof. A.McCorquodale for patient guidance offered throughout this work, and to Prof. T.W. McDonald for helpful advices during this study. The author is grateful to Dr.A.K.Menon for his help in setting up computer programmes. Thanks to Messrs. O.Brudy,P.Feimer D.K.Liebsch and G.Michalsczuk.

The author is grateful to Dr.J.F.Leddy, President, University of Windsor and the National Research Council for the financial support given.

ABSTRACT

This paper presents the results of an experimental study of the transverse curvature effects on the turbulent boundary layers formed on the outside surface of cylinders. Tubes of different diameters were aligned with their axis parallel to the flow of air or water. Velocity profiles were measured in the boundary layer at different stations along the axis of the cylinders with pitot and pitot-static tubes. The cylinders were tested in a wind tunnel at two different flow speeds, viz: 26 ft./sec. and 57 ft./sec. A similar experiment was conducted in a water tunnel with flow speeds of 2 and 2.7 ft./sec. The cylinder diameters varied from 1.25 in. to 0.25 in. and the Reynolds numbers based on cylinder diameters were in the range of 3560 to 30800.

It was found that in the shape of the velocity profiles no significant differences existed between the boundary layers that formed in water and those that formed in air. A comparison of the displacement thicknesses and the momentum thicknesses of the boundary layers in water and air also led to the same conclusions.

It was found that the velocity profiles of the turbulent boundary layers were affected by transverse curvature. A general power law of the form

$$u/U = (y/\delta)^{1/n}$$

where U = free stream velocity
u = velocity at any point in the boundary layer
y = distance perpendicular to the flow measured from the surface of the cylinder
δ = thickness of the boundary layer

was found to be valid for the turbulent boundary layer velocity profile. The exponent 1/n in the above relation decreased with increasing transverse curvature. From the different cylinders tested the following relation between the radius of the cylinder and n was obtained:

$$(n-7)\ r^{1.26} = 0.62$$

where r is the cylinder radius in inches.

The boundary layer characteristics were also found to be affected by transverse curvature. The boundary layer thicknesses and displacement thicknesses decreased with increasing curvature. Momentum thicknesses and shear stress coefficients increased with curvature.

This study also pointed out that a single inner law velocity profile is not valid for all curvatures. It indicated that each curvature has its own inner law for the boundary layer.

CONTENTS

LIST OF ILLUSTRATIONS

NOMENCLATURE

a	Radius of cylinder
C, k_1, k_2	Constants
L	Total length of cylinder
r	Radius measured from the axis of the cylinder
u	Velocity in the axial direction
U	Free stream velocity
x	Coordinate in the axial direction measured from the leading edge of the cylinder
y	Coordinate in the radial direction measured from the surface of cylinder, $y = r-a$
v	Velocity in y-direction
ν	Kinematic viscosity
ρ	Mass density of fluid
τ	Shear stress in the boundary layer
τ_a	Shear stress at the surface of the cylinder
δ	Boundary layer thickness
Re_a	Ua/ν
Re_x	Ux/ν
u_τ	$(\tau_a/\rho)^{1/2}$
u^+	u/u_τ
y^+	yu_τ/ν
c	Local friction coefficient
c_f	Average friction coefficient
k	Kärman constant
$1/n$	Index of the power law

1. INTRODUCTION

Most flows that occur in practice are turbulent and the turbulent boundary layer is responsible for the large drag forces experienced by moving objects. The apparent stresses created by turbulence in fluid flow constitute most of the resistance encountered by flow in a pipe.

The turbulent boundary layer has been a topic of great interest since 1924 when Burgers (1) and Zignen (2) published their works on boundary layer transition. The flat plate boundary layer has been studied quite extensively and the boundary layers on many other kinds of surfaces are being studied.

Transverse curvature here denotes the curvature in a plane normal to the flow direction. Fundamental information about the transverse curvature effect is needed in the calculation of friction on various moving objects such as ships and submarines. In this investigation the turbulent boundary layers on circular cylinders of various diameters were studied experimentally.

2. SURVEY OF LITERATURE

The studies conducted by earlier investigators are classified according to the nature of their works. Most of the earlier works could be arranged in two sections: experimental studies and theoretical studies. Investigations that include both theoretical and experimental studies are discussed in both sections.

2.1. Experimental work

The first work on transverse curvature effect was published as early as 1924 by Kempf (3). He made an experimental study of the effect of transverse curvature using cylinders of different lengths. He determined average skin friction coefficients at different flow speeds.

Karhan (4) conducted experiments with pontoons of different roughnesses in 1952. By combining his results with the earlier results obtained by Kempf (3), he derived a curvature correction for the friction coefficient.

Hughes (5) studied the effect on a one inch diameter cylinder and predicted an increase in resistance with an increase in the length radius ratio. His experiments were affected by pressure gradients of unknown magnitude.

Richmond's (6) experiments were performed on a one

inch diameter cylinder and a wire of 0.024 inch diameter. They were mounted under tension in a wind tunnel. The velocity profiles were measured using pitot static tubes and hot wire anenometers, at various axial distances. The skin friction values were calculated and an increase over flat plate skin friction was predicted. The inner laws for the boundary layer were derived and plotted as u^+ vs. $y^+(1 + y/2a)$. The calculation of skin friction was valid only when the laminar sublayer thickness is negligible in comparison to the radius of the cylinder. So considerable error was introduced in the friction values and the inner law velocity profiles of the wire. The velocity measurements in the boundary layer on the wire was carried out using a hot wire which was supposed to be calibrated for mean flow. The velocity profile obtained was not found to obey a power law.

Yu (7) used a two inch diameter cylinder for his study. The radius Reynolds numbers were 15,000, 30,000, and 45,000. He used a Preston tube for skin friction measurements with the calibration given by Landweber and Siao (22). Using the results obtained the inner laws and the outer laws of the boundary layer were predicted.

0	$\leq$	y^+	$\leq$	30	$u^+ = y^+$
30	$\leq$	y^+	$\leq$	300	Inner laws, (eqn. 10, ref. 7.)
300	$\leq$	y^+			Outer laws, (eqn. 12, ref. 7.)

Yasuhara (8) studied the effect of curvature on

laminar and turbulent boundary layers that formed on a 20 mm. diameter cylinder. The study of the turbulent boundary layer indicated the general trend of the boundary layer characteristics although the results could not be used for quantitative prediction.

Bonsignore (9), from his studies of a 1.25 inch diameter cylinder, predicted a change in the shape of the velocity profile from that of the flat plate. He indicated a variation of the index of the power law with curvature.

Singh (10) in his study of wall jets used cylinders of 10, 3.5, and 1 inch diameters. Using a Preston tube the friction coefficients were determined and the inner laws were calculated and plotted.

Shirtliffe (11) measured the turbulent boundary layer velocity profiles on 1/4, 3/8, 1/2 and 1 inch diameter cylinders of two feet length, mounted in a wind tunnel. Local friction coefficients were predicted assuming the results of Sparrow (20).

Venkatasubramanian (12) found from his experimental study that the universal velocity profile is not acceptable for the curvature case.

2.2. Theoretical work

Landweber (13) assumed a one-seventh power law velocity distribution and the Blasius empirical shear stress formula for the calculation of curvature effect. The variation of power law with curvature was not known at that time

and no effort for such a correction was made. The momentum thickness for the boundary layer on the cylinder was defined and a differentiation of the momentum thickness with the assumed power law led to the coefficient of friction. The flat plate skin friction was also calculated similarly and the ratios of skin frictions were obtained.

In his study, Eckert (14) made the same assumptions as Landweber (13). His work was an extension of the work of Landweber into the compressible flow region. Boundary layer thickness, displacement and momentum thicknesses, and skin friction coefficients were calculated and plotted for different curvatures and different Mach numbers.

Karhan (15) selected a generalized power law of the form $u/U = (y/\delta)^{1/n}$ for the velocity profile and calculated skin friction in the same way as Landweber (13) and Eckert (14). He also overlooked the change in the power law due to curvature. However, the assumptions of Landweber, Eckert and Karhan could be justified to some extent since their studies were oriented toward the calculation of drag forces on ships where the curvature is too small to cause any appreciable change in the power law.

Telfer (16) derived the formula for average skin friction

$$c_f = 0.0012 + \left[\frac{0.07}{(a/L)^{1/3}} + 0.34\right]\left[\frac{\nu}{UL}\right]^{1/3}$$

By this formula c_f decreases with length at fixed radius and increases with curvature for fixed length.

Ginevskii and Solodkin (17) assumed a shear stress distribution of the form

$$\tau = \frac{a\tau_a}{r} \qquad \text{for the entire boundary layer}$$

$$\tau = \mu \frac{du}{dy} \qquad \text{for the laminar sublayer}$$

and $$\tau = \rho k^2 y^2 \left|\frac{du}{dy}\right| \frac{du}{dy} \qquad \text{for the turbulent core}$$

It was further assumed that the laminar sublayer extended up to $y^+ = 11.5$. Velocity profiles were established for convex and concave surfaces.

Sasjima, Takaji and Tanaka (18) studied the curvature effect with the same assumptions as Ginevskii and Solodkin (17), except that they assumed the shear stress to be constant for any radius within the laminar sublayer. The laminar sublayer was assumed to extend only up to $y^+ = 6.82$. The error introduced by the assumption of a linear relation between u and y was limited by assuming a smaller thickness; but at the same time more errors were introduced by this, since the turbulent core was assumed to extend to $y^+ = 6.82$. Velocity profiles and friction coefficients were calculated and compared with flat plate values.

Reid and Wilson (19) also used the Karman-Prandtl mixing length theory with 0.4 as the von Karman constant k. They assumed the distribution of shear stress

$$r\tau = a\tau_a$$

and predicted velocity profiles for the laminar sublayer and the turbulent core. The results included friction

coefficients for smooth and rough cylinders.

Sparrow, Eckert and Minkowycz (20) predicted the friction coefficients by assuming a distribution for the eddy diffusivity. They assumed different distributions for regions near the wall and away from the wall. They also assumed the relation

$$r\tau = a\tau_a$$

The inner law was calculated.

Rao (21) assumed $r\tau = a\tau_a = \mu \frac{du}{dy}$ for the laminar sublayer and the velocity profile for this region was obtained as

$$u/u_\tau = \frac{u_\tau a}{\nu} \log (r/a)$$

From this finding he inferred that the velocity profile for the turbulent core was:

$$\frac{u}{u_\tau} = \frac{1}{k} \log \left[\frac{u_\tau a}{\nu} \log \frac{r}{a}\right] + 5.75$$

The laminar sublayer was supposed to extend up to $y^+ = 5$.

Venkatasubramanian (12) (see Section 2.1) in his theoretical analysis of transverse curvature assumed the universal velocity profile, and predicted skin friction. The friction coefficient was shown as a function of Rea and Rex.

2.3. Remarks

Landweber (12), Eckert (14), and Karhan (15), in their works assumed that the power law was unaffected by curvature. This assumption was not supported by any previous

work, and if the power law is affected by curvature, the calculations of skin friction made by these investigators would not be exact. The study of Bonsignore (9) in 1966 indicated such an effect although his work did not explain completely the curvature effects on the power law. The present investigation was undertaken to determine the exact effects of different curvatures on the power law.

3. EXPERIMENTAL STUDY

Experiments were conducted to determine the boundary layer velocity profiles in a water tunnel as well as in a wind tunnel. The water tunnel was fabricated for the purpose of this study and the wind tunnel was the existing low speed wind tunnel of the Mechanical Engineering Laboratory.

3.1. Water tunnel set up

The water tunnel had two main sections; an inlet section and a test section (Fig. 1).

The inlet section was made out of 3/4" thick plywood and was 8 ft. long and 11" x 11" inside. The four corners of this section were made watertight by applying resorcinol glue. The connecting piece shown in Fig. 1, was 15" x 20" and was used to connect the inlet section of the tunnel to the outlet of a head tank. Two screens were fixed inside the tunnel so as to make the velocity profile more uniform. The screen 1 consisted of a two inch thick resilatex screen supported both sides by two metallic screens. Screen 2 was a thin metallic screen. Near the downstream end of this section a flow straightener was fixed as shown in Fig. 1. The flow straightener made out of sheet metal had 1" x 1" square cells, 2 inches long. This piece served to stop any

secondary flow starting in the inlet section.

The test section (Fig. 1.), made out of $\frac{1}{2}$" thick plexiglass, was 6 ft. long and 11" x 11" inside (static pressure taps were located every 6" on one side). There was a window at the upstream end of this section. The window gave access into this part of the tunnel. A watertight shutter was provided for the window. The inside surface of this shutter was even with the inside surface of the tunnel wall when the window is closed. A slot $\frac{1}{4}$" wide was cut at the top of the working section. The slot was $5\frac{1}{2}$ ft. long and was located exactly at the center as shown in Fig. 2. The slot was provided with a cover made out of 6 inch long plexiglass pieces. The lower surface of the cover pieces was flush with the inside tunnel surface.

An adjustable gate was fixed at the downstream end of the test section. This wooden gate had two parts, a fixed gate and a movable gate. Each was made out of rectangular bars placed horizontally on a frame with gaps between them. In the fully open position the bars of the fixed and movable gates coincided leaving about half of the area open. When the movable gate was pulled upward, the open areas were gradually closed by the bars in the movable gate, thereby achieving a continuous variation of the area open for the flow.

The water for the experiment was supplied from the sump below the floor by a centrifugal pump with an approximate capacity of 3000 g.p.m. The pump was driven by an

induction motor of 40 H.P. The water from the pump was carried in a one foot diameter pipe with an adjustable valve. A magnetic flow meter recorded the flow rate in g.p.m. The pipe discharged the water into a head tank. The flow diagram is shown in Fig. 1.

The tank was 4' x 2' x 5'. It was made of wood. There was a 11" x 11" opening at the bottom which served as the outlet. A rounded outlet was provided to give a smooth flow into the tunnel. The pipe which discharged water into the tank extended to the bottom to reduce air entrainment.

3.2. Auxiliary equipment

Two rigid metallic supports were erected at the downstream end of the test section and these two supports held the test cylinder firmly with the cylinder axis coinciding with the center line of the tunnel.

Thin wires of 25 thou. diameter were fixed to the test tubes at the leading edge. The wires passed through the tunnel wall and the ends were connected to four turnbuckles which were fixed on one end. The turnbuckles permitted minor adjustments of the test cylinder alignment. The test cylinder was aligned along the center of the tunnel with reference to the tunnel walls.

The traversing mechanism shown in Fig. 2. included a runway made of aluminium and a carriage for the pitot tube which could be moved along the runway. The runway was fixed to the top of the tunnel in such a way that the pitot tube

lay in the vertical plane of the centerline of the test cylinder. The pitot tube passed through a cover piece fitted in the slot of the tunnel wall. Turning of the handle, shown in Fig. 2., caused the pitot tube to move up or down, and the pitot tube position could be read accurately to 0.001". The pitot tube positions were read with reference to an initial reading taken when the pitot tube touched the cylinder surface. The slot and the runway helped to fix the pitot tube at any location along the axis of the test tube.

3.3. Wind tunnel set up

The wind tunnel used was the closed circuit low speed wind tunnel of the Mechanical Engineering Laboratory. The working section was 30" x 30" and 25 ft. long. The top wall of the wind tunnel was preadjusted to give zero pressure gradient. The tunnel was run by a 20 H.P. variable speed induction motor.

Two rigid metallic supports, similar to the supports used in the water tunnel, were used to hold the test cylinders. The supports were one foot apart and were fixed to the tunnel wall at the downstream end of the test section of the tunnel. The overhanging portions of the test cylinders were supported by small wires of 25 thou. diameter. The arrangement is shown in Fig. 3. The turnbuckles shown in the figure were helpful in small adjustments of the test cylinder while aligning these tubes with the centerline of the tunnel.

The traversing mechanism consisted of the same runway and carriage used in the water tunnel. A vertical stem was fixed on the carriage on which the probe could be supported and the traversing could be done. In this set up a pitot-static tube was held horizontally, in the plane of the axis of the test cylinder. The pitot-static tube had an inside diameter of 20 thou. for the total pressure tapping. To avoid any effects of the traversing mechanism on the readings, a parallel bar was fixed to the pitot-static tube and this bar was held between the collars of the traversing mechanism. By doing so, the pitot-static tube was placed several inches upstream of the stem of the carriage. A flexible shaft was fixed to the handle of the traversing mechanism, as shown in Fig. 3., and the other end of this shaft passed through the tunnel wall. From this end traversing could be done, and the exact position of the probe could be read through the transparent plexiglass windows of the wind tunnel. The total and static pressure taps of the probe were connected to a Lambrecht manometer. The manometer directly indicated the dynamic pressure.

The traversing mechanism and the test cylinder were connected with a flashlight cell and a millivolt meter in series. When the probe was in contact with the surface of the cylinder, the volt meter registered an electric potential. This was used to take the initial reading when the probe was touching the cylinder.

3.4. Experimental Procedure

A. Water tunnel experiment

The cylinders tested in the water tunnel were 1.25", 3/4", and 1/2" in diameter. They were 6 ft. long aluminium tubes. The outside surface of the tubes was polished and at the leading edge the inside of the tube was tapered which gave a sharp leading edge. The inside of the tube was kept open for the flow and the sharp leading edge divided the flow without separation from the outside surface at the leading edge.

Fig. 4. specifies the coordinate system used for this experimental study. Velocity profiles were measured at different stations located along the axis. The stations were from x = 1 ft. to x = 5 ft. at 1 ft. intervals. A pitot tube of 50 thou. inside diameter was used for measuring the total pressure. The static pressures indicated by all the wall taps were found to agree with the static pressure obtained from a pitot-static tube, and so one of the wall taps was used for measuring the static pressure. The pitot tube was brought in contact with the cylinder for the first reading. Later on readings were taken at 25 thou. intervals till 0.1 inch ordinate and then at 50 thou. intervals.

Experiments were conducted at two different flow speeds of approximately 2.2 and 2.7 ft./sec. Higher velocities could not be obtained since the height of the head tank was limited. The water level in the tank was shown by a glass tube on the tank wall. The experiment was

conducted only when the water level in the tank remained constant and the magnetic flow meter indicated constant flow rate into the tank. In other words, a constant flow rate through the tunnel was maintained during the experiment.

B. Wind tunnel experiment

Three cylinders of 1", $\frac{1}{2}$" and $\frac{1}{4}$" diameters were tested in the wind tunnel. They were 10 ft. long aluminium tubes. The tubes were prepared in the same way as the tubes used in the water tunnel and were with the same type of leading edge.

The velocity profiles were measured with a pitot-static tube at stations located at axial distances of 1 to 8 ft. The stations were at 1 ft. intervals as in the previous case. Readings were taken at 15 thou. intervals till 60 thou., 25 thou. intervals till 0.1 inch and 50 thou. intervals for the rest of the boundary layer thickness.

The flow speeds used for the experiment were approximately 26 ft./sec. and 57 ft./sec. Since the maximum speed allowed for the driving motor of the tunnel was limited to 12000 r.p.m., higher velocities could not be achieved for the experiment. The temperature remained more or less constant at 75°F while the experiments were carried out.

3.5. Precautions taken

Before the experiments were conducted, the water tunnel was run without test cylinders and the velocity profile was measured from top to bottom. The profile was found to

be symmetrical about the centerline and the thickness of the boundary layers on the walls was about 1 3/4". A horizontal traversing from wall to wall was not possible and the profile was not tested in this direction. It was found by the vertical traversing that apart from the boundary layers on the walls, the rest of the area had an approximately uniform velocity.

The water tunnel was also tested for any major eddies. A dye was injected from the side at the upstream end and the flow pattern was observed. The test confirmed that there were no eddies in the flow.

Symmetry of flow around the cylinder was checked by measuring the velocity profile along three different radial paths. This was done in the wind tunnel. No such check could be made in the water tunnel experiment.

A measurement of the wind tunnel turbulence was conducted at the two speeds at which the experiments were carried out. The percentage of turbulence was calculated for each speed from hot wire anemometer readings and they were :

0.328 for 27 ft./sec.

0.624 for 58 ft./sec.

To avoid the error in y-ordinate due to the clearance between the different screw threads in the traversing mechanism, the handle was rotated only in one direction while traversing.

4. RESULTS AND DISCUSSION

4.1. Velocity profiles

A. Velocity profiles for flat plate

The flat plate velocity profiles were not studied in this investigation since the 1/7th power law is generally accepted for the range of Reynolds numbers used. So for the flat plate the 1/7th power law was assumed.

B. Velocity profiles for the cylinders

The velocity profiles obtained for different cylinders at different stations are shown in Figures 5 to 10.

For the velocity profiles the boundary layer thickness was fixed as the y-ordinate when $u/U = 0.99$. This limit was taken from an average curve computed from the observed data. The boundary layer thicknesses are entered in Table 1. When the boundary layer thicknesses were compared with those of the flat plate derived from 1/7th power law, it was found that the transverse curvature caused a reduction in boundary layer thickness. This effect is shown in Fig. 11. The flat plate boundary layer thickness was the maximum. The boundary layer thickness went on decreasing with curvature and $\frac{1}{4}$" diameter cylinder had the least thickness.

The velocity profiles obtained for each cylinder

were found to bear similarity. That is, the nondimensional velocity-profiles remained unchanged for each cylinder irrespective of the axial distance. This is shown in Fig. 12 and Fig. 13. In most cases the similarity started from an axial distance of 4 ft. from the leading edge, even though in a few cases similarity was obtained even at 3 ft. distance. All velocity frofiles obeyed the relation $u/U = (y/\delta)^{1/n}$. For each test cylinder a value of n was found to remain constant as shown in Fig. 13, irrespective of flow velocity or axial distance. At this point it is interesting to note the paper (24) by Nikuradse. He related n to Reynolds number. The Reynolds number effect on n, which he predicted was very small and the variation of flow speed achieved in the experiments was not sufficient enough to indicate any such effect.

In Fig. 14 the nondimensional velocity profiles are shown for different cylinders. The flat plate velocity profile according to the 1/7th power law is also shown. The velocity profiles of the cylinders could be seen to have larger velocity gradients at small y-ordinates and smaller gradients at large y-ordinates compared to the flat plate profile.

It was observed that in the region of similarity the value of n depended very much on the radius of the tube (See Fig. 15). n increased with curvature. The experiments conducted both in the water tunnel and the wind tunnel supported this effect and also the values of n obtained in both cases

showed very good agreement.

Diameter in inches	1.25*	1	0.75*	0.5	0.5*	0.25
n	7.7	8	9.4	10.9	10.9	15.3

(*Tests were conducted in water tunnel)

From the relation $u/U = (y/\delta)^{1/n}$ the value of n was calculated for each observed data and the average n was found for each station. These values are shown in Table 2. The average of these values of n was calculated for stations located in the region of similarity for each cylinder and the new values are shown in the table above.

The above table indicated the existence of a relation between n and radius a. Since the experiments failed to indicate any effect of flow speed on the value of n, in no way could the radius of the cylinder be expressed non-dimensionally. So a relation between n and radius was obtained keeping a in dimensional form. A preliminary investigation led to the relation:

$$(n-7)\, a^{k_1} = k_2$$

The relation had these obvious advantages:

(1) $a \to \infty$ $n \to 7$ [Flat plate and 1/7th power law]

(2) $a \to 0$ $n \to \infty$ [The object vanishes and the boundary layer also vanishes]

Using the experimental values of n and a the best values of k_1 and k_2 were determined simultaneously by using the program of Appendix 1. in an I.B.M. 360-40 computer. The final

relation was:

$$(n-7)\, a^{1.26} = 0.62 \qquad a \text{ in inches}$$

In Fig. 16. the final relation of n and radius a shows very good agreement with the experimental points. A few values of n available from other experimental investigators like Yu (7) and Richmond (6) also indicated good agreement. The velocity profiles measured by other investigators could not be compared due to nonavailability of data.

The velocity profiles obtained at stations in the first 4 ft. of axial distance showed a variation of n with x-distance. It was observed that n gradually decreased with axial distance. But the results were not convincing enough to make positive conclusions. However the obtained values of n are shown in Fig. 17.

4.2. Displacement thickness

The definition of the displacement thickness used for the flat plate was not applicable here since as the radius changes, a variation of circumferential area is taking place. So the new definition used for the displacement thickness is:

$$\delta_1 = \int_0^{\delta} (1 - u/U)\,(1 + y/a)\, dy \quad \text{(see Appendix 2.)}$$

Table 3. shows the displacement thicknesses obtained for each cylinder at different stations. The displacement thicknesses are found to decrease with curvature as seen in Fig. 18. This decrease was caused by the curvature effect on the velocity profile. Although the effect of the curvature

term y/a in the definition was to increase the value, the net result was a decrease.

4.3. Momentum thickness

Just as in section 4.2. the new definition used for the momentum thickness is:

$$\delta_2 = \int_0^{\delta} (u/U)(1 - u/U)\ (1 + y/a)\ dy$$

Table 4. shows the momentum thicknesses calculated by the above definition. In momentum thickness the effect of the curvature term y/a was quite significant. The curvature effect on the velocity profile caused the momentum thickness to decrease from the value of flat plate. But this decrease is gradually overcome by the effect of the curvature term in the definition. Fig. 19. shows the total curvature effect on the momentum thickness.

4.4. Skin Friction

Measurements of local skin friction coefficients were conducted by Yu (7) and Singh (10), using Preston's method of using a calibrated stagnation tube. The calibration used by Yu was obtained from Landweber and Siao (22) which was based on the logarithmic law of the flat plate boundary layer. The assumption that the logarithmic law of the flat plate was valid for the boundary layer with transverse curvature was questionable. The local skin friction coefficients were predicted and as expected the inner laws calculated using these friction values turned

out to be different from the logarithmic law. However the errors were not considerable since the curvatures involved were small. From this it was plain that for higher curvatures the errors could be considerable. Moreover the errors caused could be different in magnitude for different cylinders. So Preston tube with the available calibrations could not be used in this study.

Many previous investigators based their calculations of skin friction on some form of inner law. But again, comparing the inner laws obtained by different people by different means, one might infer that a single general inner law was not applicable for all curvatures. At least one could definitely question the idea of a single inner law velocity profile. In this light the calculation of friction based on a velocity profile was also questionable.

The only way open was to calculate friction using momentum thickness. The average friction coefficient could be obtained from the momentum thickness determined from the experimental velocity profile. But the local friction coefficients found by the slope of the momentum thickness at each point are not acceptable since the measurement of a very small slope cannot be very accurate. This difficulty was overcome by using the power law obtained by experiment with the following analytical approach.

$$u/U = (y/\delta)^{1/n} \qquad 1$$

$$u_\tau = \sqrt{\tau_a/\rho} \qquad 2$$

Equation 1 was nondimensionalized using equation 2 to get equations 3 and 4.

$$u/u_\tau = C \left\{\frac{yu_\tau}{\nu}\right\}^{1/n} \qquad 3$$

$$\tau_a = \rho\, C^{-2n/(1+n)}\, U^{2n/(1+n)}\, (\tfrac{\nu}{\delta})^{2/(1+n)} \qquad 4$$

from section 4-3

$$\delta_2 = \int_0^\delta (u/U)(1-u/U)\,(1 + y/a)\, dy \qquad 5$$

$$\frac{\tau_a}{\rho U^2} = \frac{C_\tau}{2} = \frac{d\,\delta_2}{dx} \qquad 6$$

comparing 5 and 6

$$\tau_a = \rho\, U^2 \frac{d}{dx} \int_0^\delta (u/U)(1-u/U)(1+y/a)\, dy \qquad 7$$

The integration in equation 7 was performed using equation 1 (see Appendix 3.). The resulting equation is as:

$$\tau_a = \rho U^2 \left(\frac{n}{(n+2)(n+1)} + \frac{n}{(2n+1)(n+1)} \frac{\delta}{a} \right) \frac{d\delta}{dx} \qquad 8$$

The expressions for τ_a in equations 8 and 4 were equated and the resulting expressions integrated with respect to x to get (Appendix 3.):

$$\delta\left(1+\frac{(n+3)}{2(2n+1)}\frac{\delta}{a}\right) = C^{-2n/(n+3)}\, Rx^{-2/n+3)} \times \left[\frac{n}{(n+2)(n+3)}\right]^{(n+1)/(n+3)} \qquad 9$$

using equations 4 and 6

$$C_\tau = 2C^{-2n/(1+n)}\, U^{-2/(1+n)}\, (\tfrac{\nu}{\delta})^{2/(1+n)} \qquad 10$$

Equations 9 and 10 were used together with experimental

results to calculate the local friction coefficients. The factors in equations 9 and 10 were determined to a good level of accuracy by experiment. So by this method the measurements of the slopes of momentum thickness which are subject to large errors were avoided.

The results obtained are shown in Fig. 20. It could be seen that the local friction coefficients of different cylinders arranged themselves in separate patterns. This further strengthened the idea of different inner laws for different curvatures. For the flat plate, the 1/7th power law agrees very well with the universal velocity profile.

$$u/u_\tau = 5.75 \log y^+ + 5.5$$

in the region $30 \leq y^+ \leq 300$. In the place of 1/7th power law other power laws with successively diminishing index 1/n with curvature were obtained in Section 4.1. This fact also pointed out that the idea of a unique inner law for all curvatures was not acceptable.

4.5. Accuracy of the results

A complete estimation of the accuracy of all results is not attempted in this section. The errors from different sources are stated and the approximate magnitude of each is indicated.

Accuracy of manometer readings	$\pm 5\%$
Alignment of test cylinder	
in wind tunnel	$\pm$ 0.05 inch
in water tunnel	$\pm$ 0.01 inch
Temperature fluctuations	$\pm$ 3 F
Corresponding fluctuations in	
absolute viscosity (for air	$\pm$ 0.4%
(for water	$\pm$ 2.3%
Fluctuations in pressure	
for air	0.6%
for water	very small
Tolerance of cylinders	$\pm$ 0.001 inch
calibration errors	$\pm$ 2%

A rough estimation of the errors in some of the derived results could be made as shown:

error in δ

$$y/\delta = (u/U)^n$$

$$\left|\frac{d\delta}{\delta}\right| = \left|\frac{dy}{y}\right| + n\left|\frac{du}{u}\right|$$

Although the dial in the traversing mechanism is marked up to 0.001", due to tolerances on different parts of the mechanism the same accuracy could not be claimed.

0.0100 inch accuracy could be safely assumed and considering the boundary layer thickness to be roughly one inch dy/y is estimated to be 0.01.

The maximum value of n could be taken as 16.

$$u^2 = kh$$

$$2\, du/u = dh/h$$

for a maximum manometer reading of 100 mm. and an uncertainty of 0.5 mm.

$$du/u = 1/2\, dh/h = .0025$$

$$\frac{d\delta}{\delta} = .01 + 16 \times .0025 = .05 = 5\%$$

In this analysis n is assumed to be accurate. This could be justified because most of the errors in the value of n are random errors and a mean of a sample of 20, will have a very small error. The only error in n which is not random in nature is due to the error in boundary layer thickness itself. This error is constant for all readings which belong to one velocity profile. So for a cylinder with 5 stations in the similarity region and velocity profiles available for 2 flow speeds, this error also could be treated as a random error with a sample size of 10. However a rough estimate of the accuracy of n will be indicated by the root mean square value of the deviations in n from the average value.

For 0.5 inch diameter cylinder:

the average value of n = 10.9

Mean of the square of deviations from this (see Table 2)

= 0.265 (for wind tunnel)

r.m.s. value = 0.515

.515/10.9 = 4.73%

For the water tunnel tests the corresponding value is

.15/10.9 = 1.4%

From equations 9 and 10 the approximate error in friction coefficient was estimated to be 15%. For this estimation the error in boundary layer thickness was assumed to be 5% and the errors in the values of n, x, and U were neglected.

5. CONCLUSIONS

The following conclusions were made from the results of this experimental study:

The velocity profiles of the turbulent boundary layers formed on the outside surface of cylinders may be closely approximated by a power law of the form

$$u/U = (y/\delta)^{1/n}$$

The shape of the velocity profiles is affected by transverse curvature. The index 1/n of the power law decreases with increasing curvature. The radius of the cylinder is found to be related to n of the power law. The relation is

$$(n - 7)\, a^{1.26} = 0.62 \quad \text{where a is in inches}$$

The boundary layer thickness and the displacement thickness decrease with curvature. In comparison to the flat plate momentum thickness, the momentum thicknesses of the cylinders decrease with curvature in the initial regions and then gradually increase with axial distance.

The local friction coefficients increase with curvature.

The u^+ vs. y^+ relation (the inner law velocity profile) does not remain constant for all curvatures.

T A B L E. 1.

BOUNDARY LAYER THICKNESS IN INCHES

X		1'	2'	3'	4'	5'	6'	7'	8'
1.25in.dia.		0.37	0.61	0.69	0.83	1.00			
0.75 ""		0.31	0 60	0.82	0.82	0.99			
0.5 ""		0.30	0.56	0.69	0.79	0.95			
1.0 "	57.87ft/sec.	0.33	0.54	0.70	0.78	0.96	1.06	1.20	1.30
	26.98 "	0.38	0.66	0.71	0.81	0.96	1.01	1.30	1.44
0.5 "	57.39 "	0.30	0.54	0.66	0.76	0.94	1.03	1.15	1.23
	26.41 "	0.34	0.59	0.70	0.80	0.96	1.03	1.20	1.30
0.25 "	57.87 "	0.29	0.50	0.65	0.72	0.86	0.95	1.00	1.07
	26.77 "	0.27	0.53	0.68	0.76	0.82	1.02	1.11	1.18

T A B L E. 2.

VALUES OF n

X		1'	2'	3'	4'	5'	6'	7'	8'
1.25in.dia.	low vel.	8.7	8.5	7.9	7.64	7.99			
	high vel.	9.0	8.4	8.1	7.82	7.36			
0.75 "	low vel.	10.9	10.5	10.0	9.8	9.4			
	high vel.	11.2	11.0	10.0	11.2	9.4			
0.5 "	low vel.	10.9	11.89	11.5	10.95	11.08			
	high vel.	12.8	11.7	11.3	10.69	11.01			
1.0 "	low vel.	10.0	9.7	9.0	7.1	7.7	8.67	8.16	7.53
	high vel.	10.3	9.5	9.1	8.65	7.54	8.87	8.13	8.43
0.5 "	low vel.	13.0	12.1	11.3	10.95	11.14	10.73	10.3	10.74
	high vel.	12.72	12.31	11.5	10.28	12.17	11.32	10.83	10.8
0.25 "	low vel.	14.6	16.5	15.2	14.84	15.22	15.54	16.51	15.9
	high vel.	18.0	16.8	15.5	15.32	16.37	15.02	14.4	14.31

T A B L E. 3.

DISPLACEMENT THICKNESS IN INCHES .

X		1'	2'	3'	4'	5'	6'	7'	8'
1.25in.dia.	(high vel. & low vel.)	0.04	0.08	0.12	0.13	0.16			
0.75 "		0.03	0.07	0.11	0.12	0.16			
0.5 "		0.03	0.07	0.09	0.12	0.16			
1.0 "	high vel.	0.04	0.06	0.09	0.12	0.16	0.18	0.21	0.24
	low vel.	0.04	0.08	0.09	0.13	0.17	0.20	0.24	0.28
0.5 "	high vel.	0.03	0.06	0.09	0.11	0.16	0.18	0.21	0.24
	low vel.	0.03	0.07	0.10	0.12	0.16	0.19	0.23	0.26
0.25 "	high vel.	0.03	0.05	0.08	0.11	0.15	0.18	0.19	0.21
	low vel.	0.02	0.06	0.10	0.12	0.17	0.19	0.23	0.25

T A B L E. 4.

MOMENTUM THICKNESS IN INCHES

X		1'	2'	3'	4'	5'	6'	7'	8'
1.25 in.dia.	(high vel. & low vel.)	0.04	0.07	0.10	0.10	0.14			
0.75 "	(high vel. & low vel.)	0.03	0.06	0.10	0.10	0 14			
0.5 "	(high vel. & low vel.)	0.02	0.06	0.09	0.11	0.14			
1.0 "	high vel.	0.03	0.06	0.08	0.10	0.14	0.15	0.18	0.20
	low vel.	0.04	0.07	0.08	0.11	0.14	0.17	0 20	0.24
0.50 "	high vel.	0.02	0.06	0.08	0.10	0.14	0.16	0.19	0.21
	low vel.	0.03	0.06	0.09	0.11	0.15	0.17	0.20	0.23
0.25 "	high vel.	0.02	0.05	0.08	0.10	0.14	0.16	0.17	0.20
	low vel.	0.02	0.06	0.08	0.11	0.16	0.17	0.21	0.23

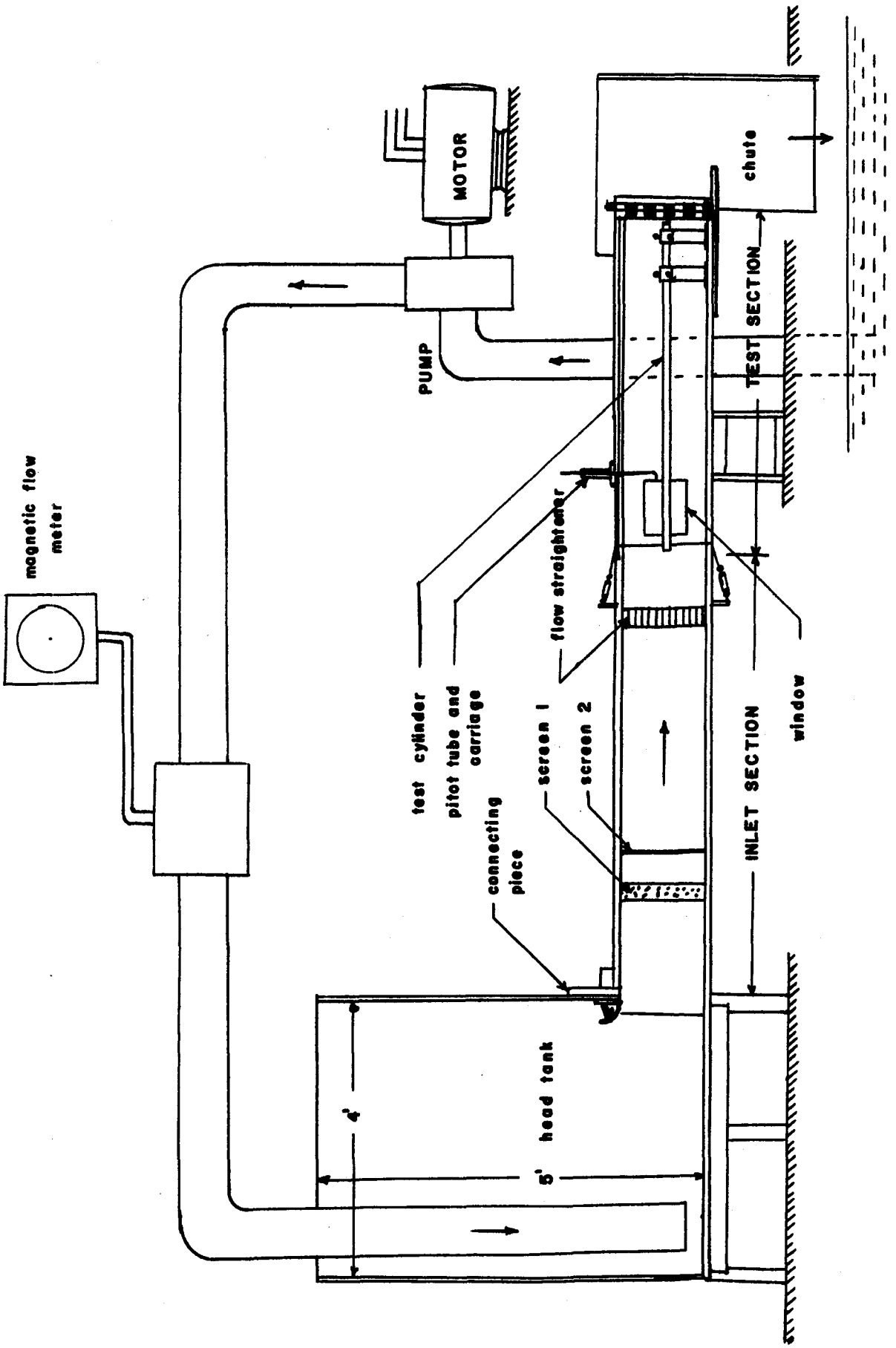

Fig. 1. Water tunnel set up

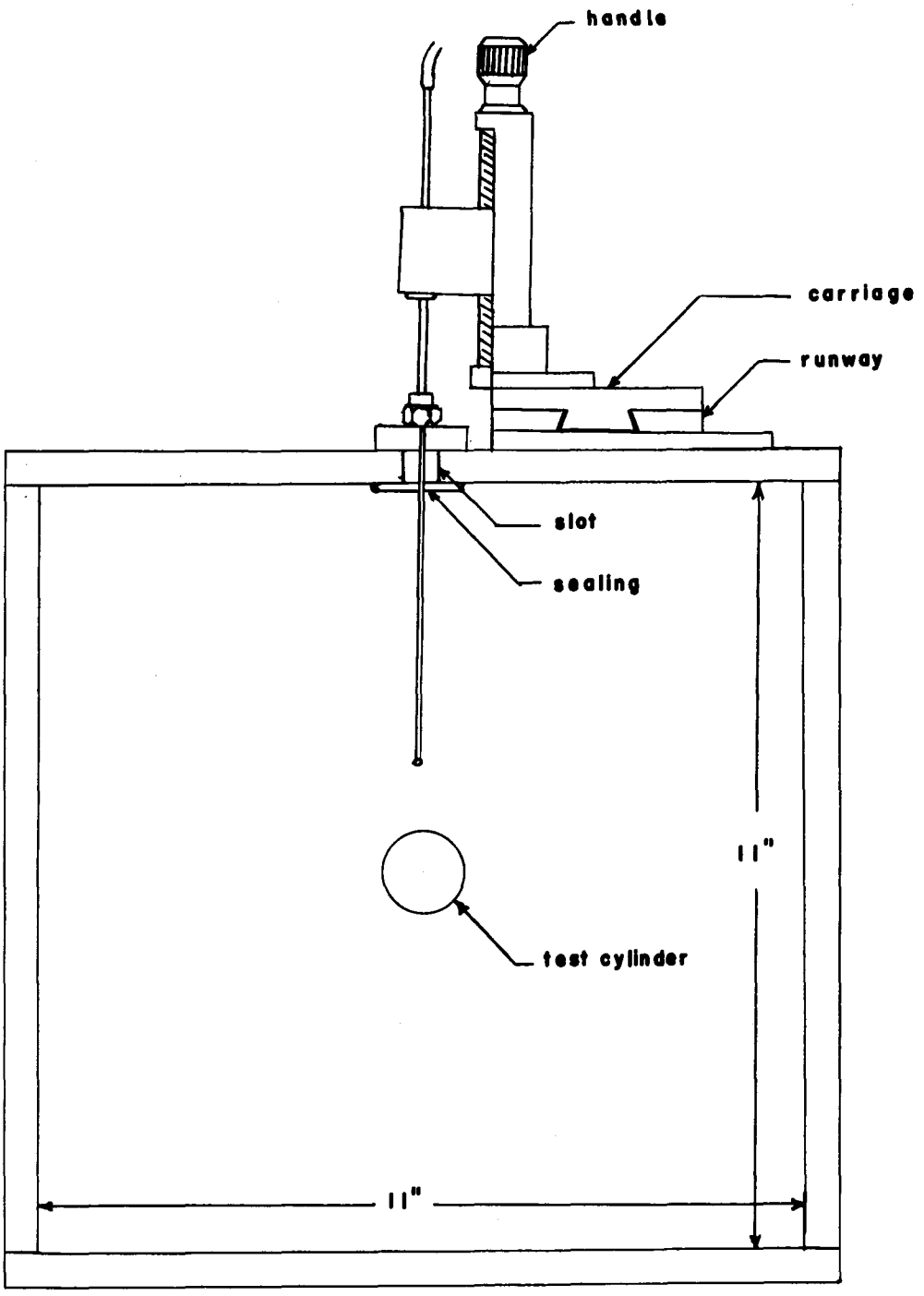

Fig. 2. Water tunnel test section

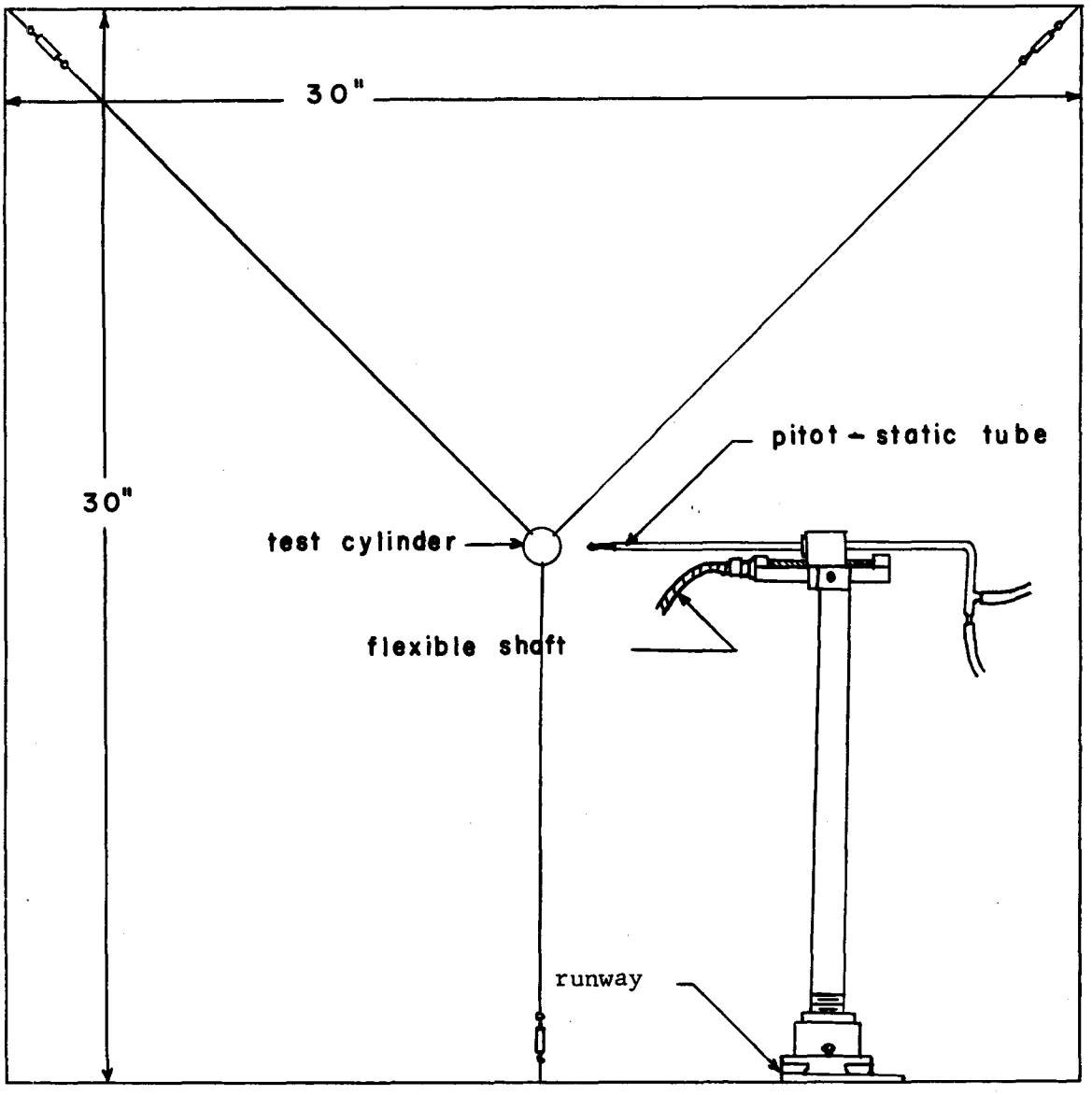

Fig. 3. Wind tunnel test section

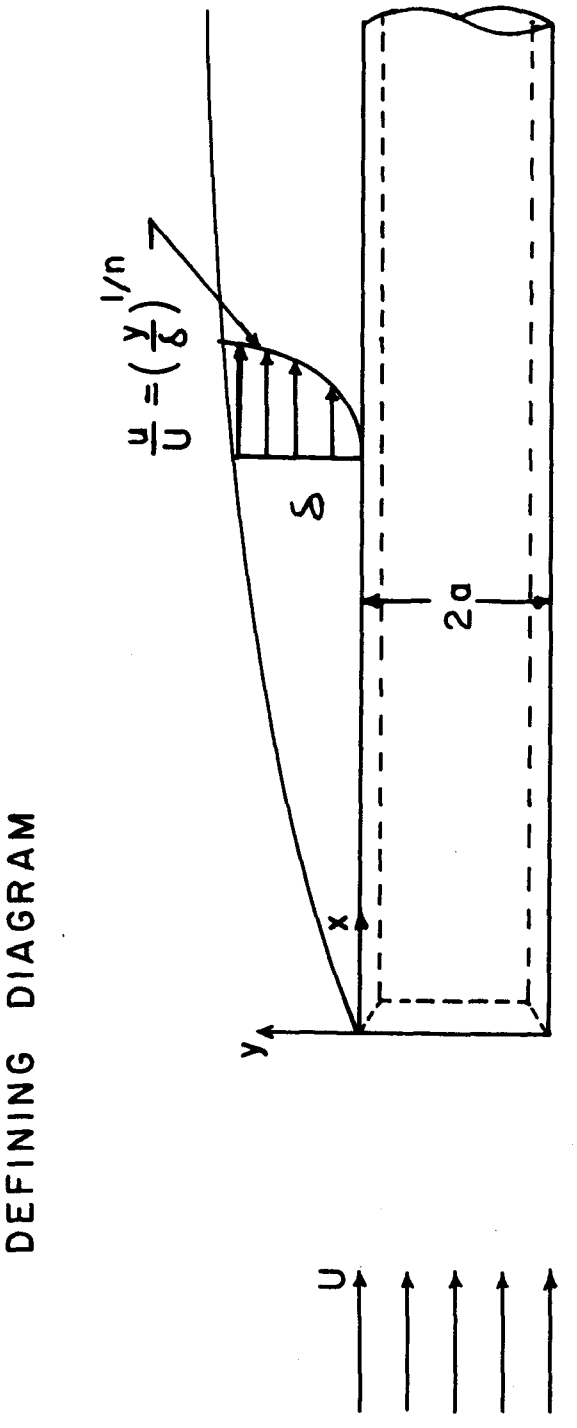

DEFINING DIAGRAM

Fig. 4.

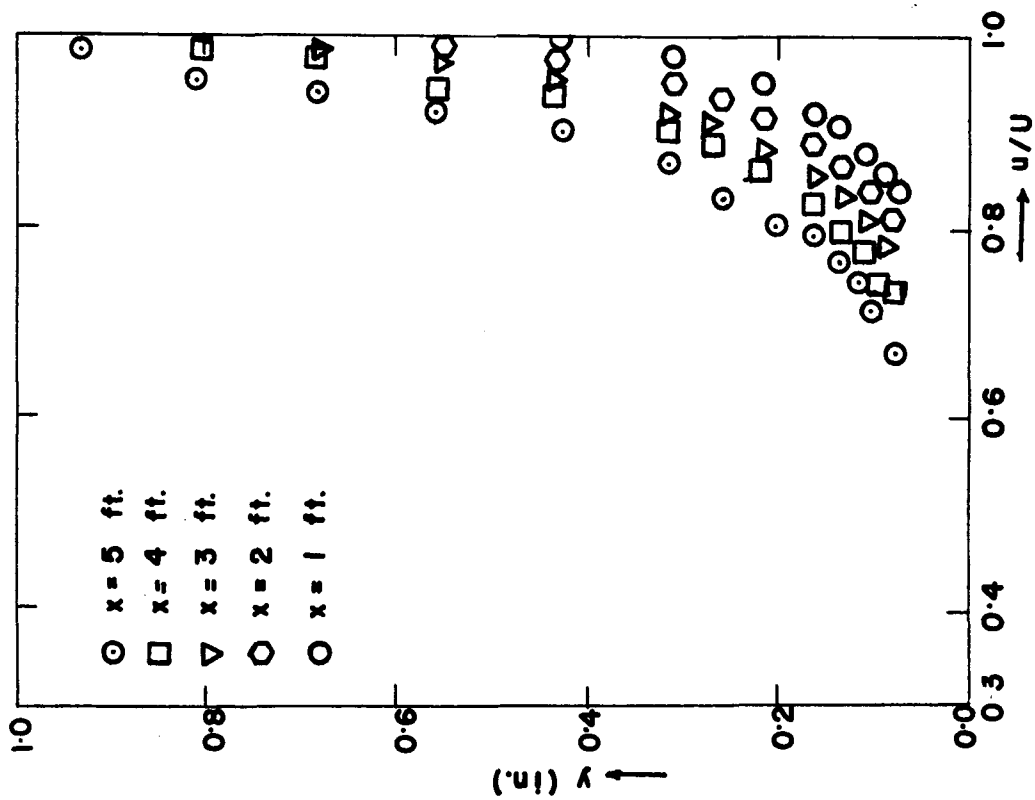

Fig. 6. Velocity profile.
0·75 in. dia. cylinder.

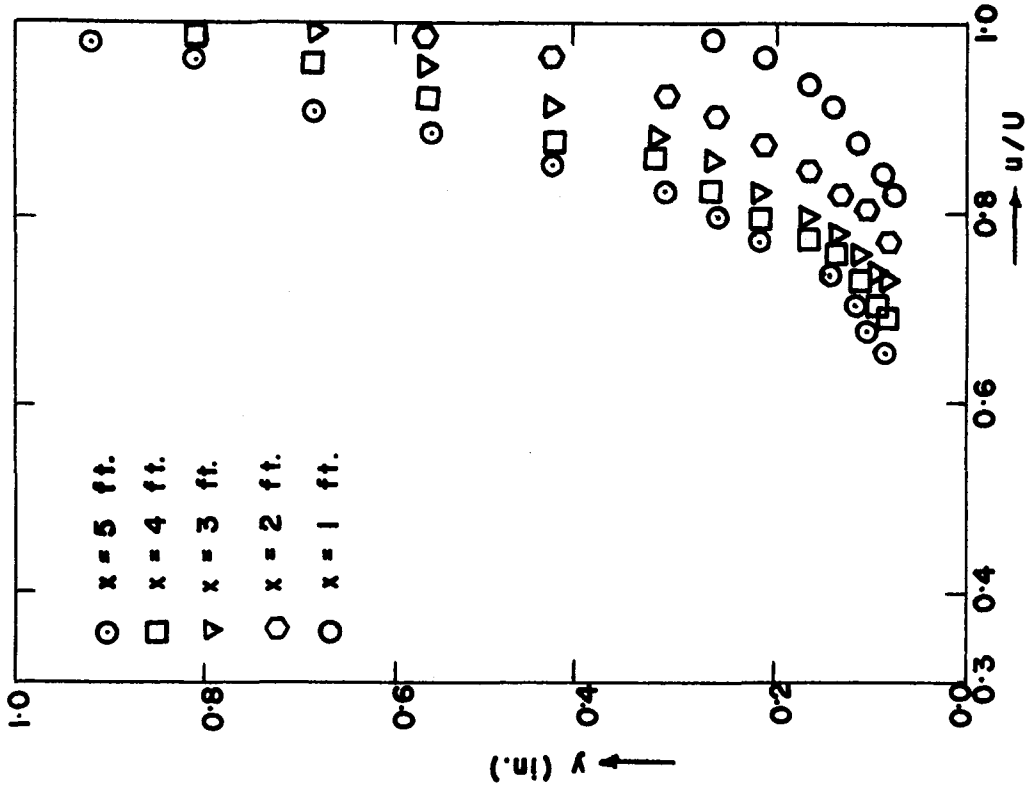

Fig. 5. Velocity profile.
1·25 in. dia. cylinder.

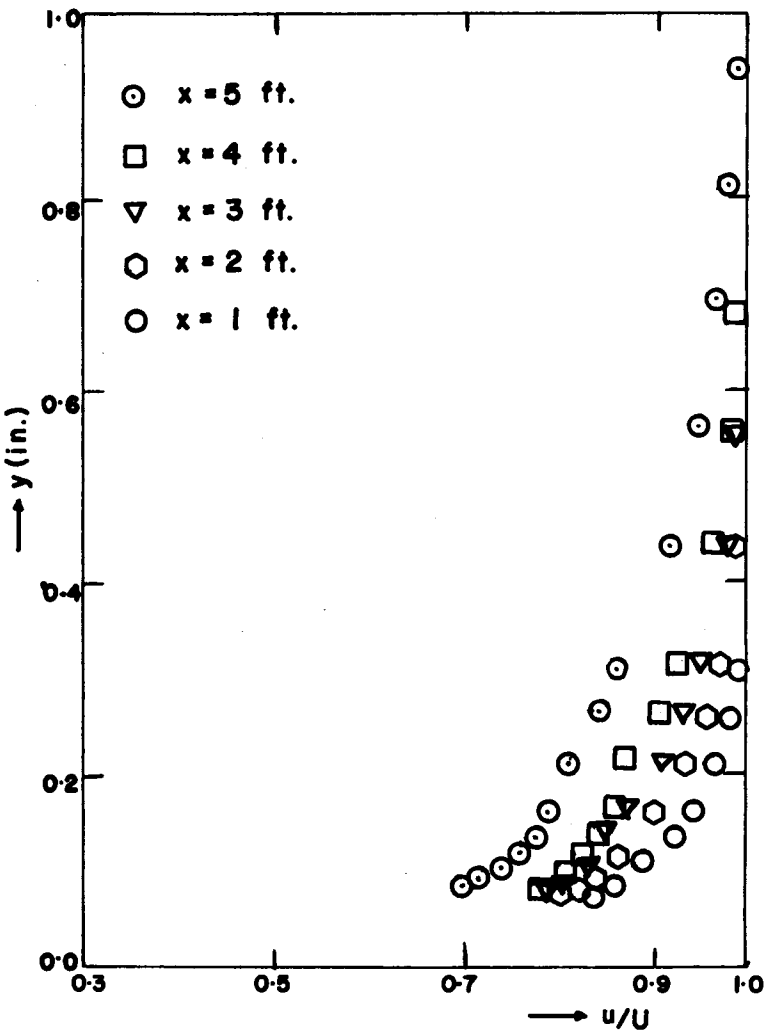

Fig. 7. Velocity profile.
0·5 in. dia. cylinder.
water tunnel.

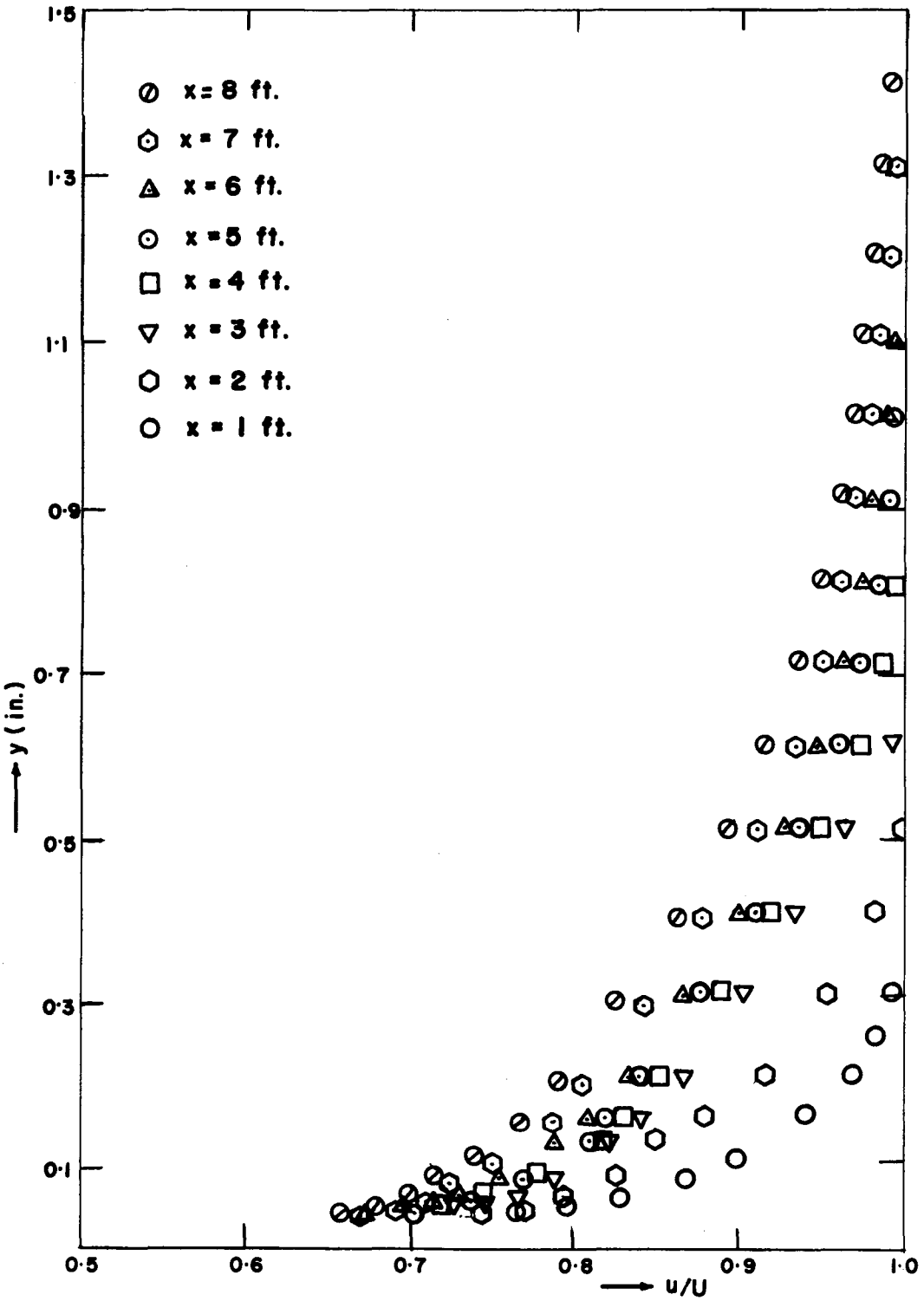

Fig.8. Velocity profile
1·0 in. dia. cylinder.

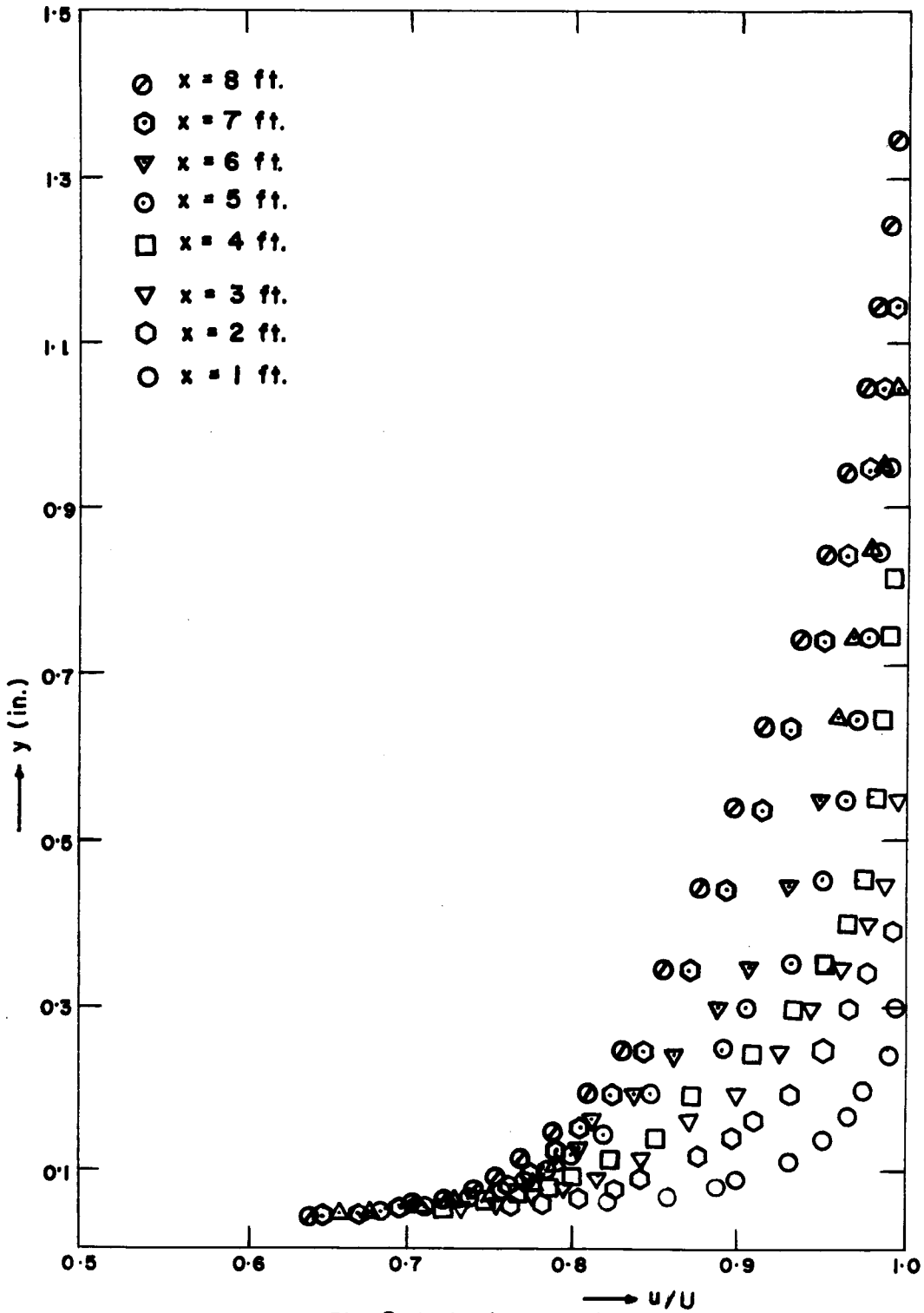

Fig. 9. Velocity profile.
0·5 in. dia. cylinder.
wind tunnel

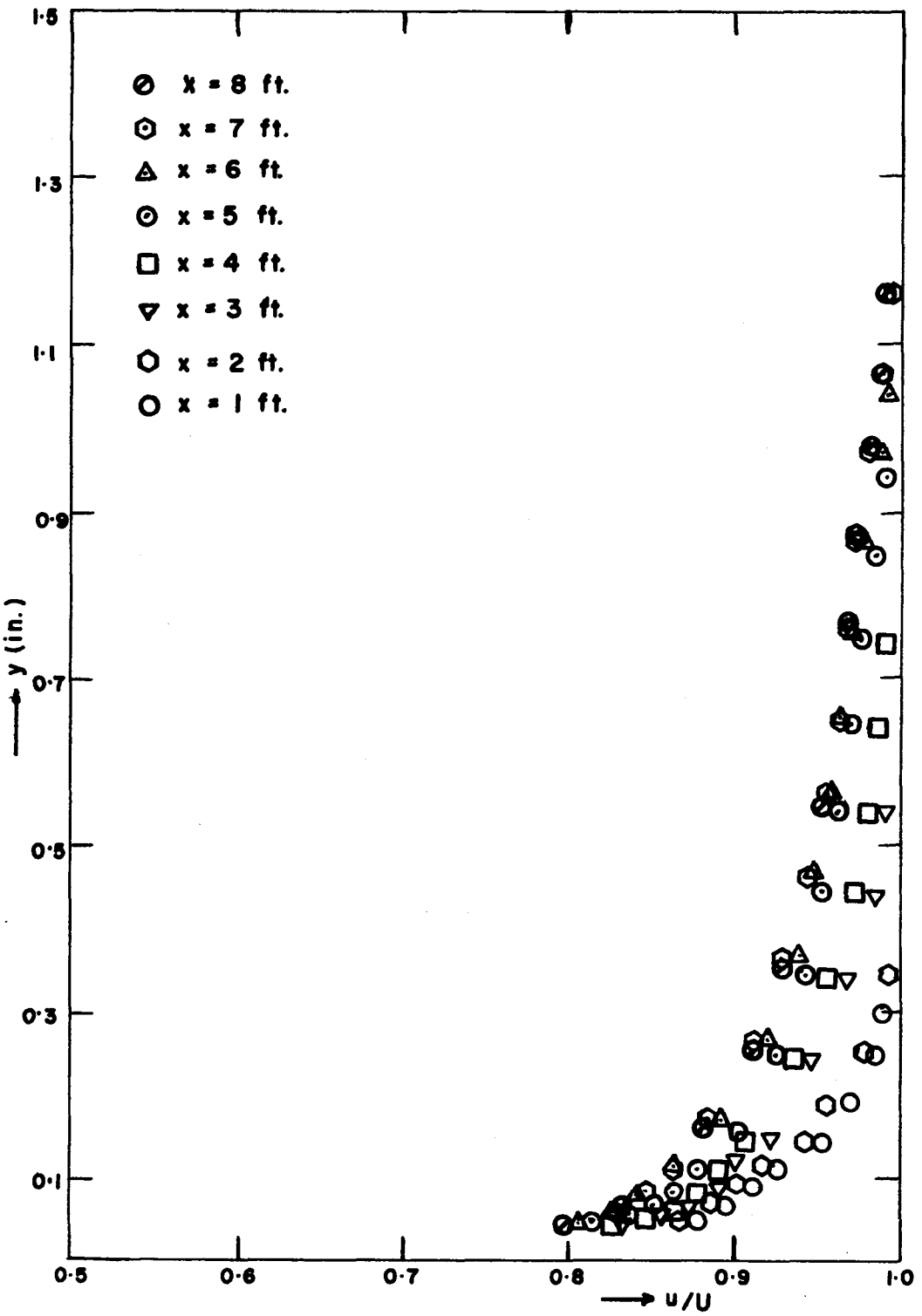

Fig. 10. Velocity profile.
0·25 in. dia. cylinder.

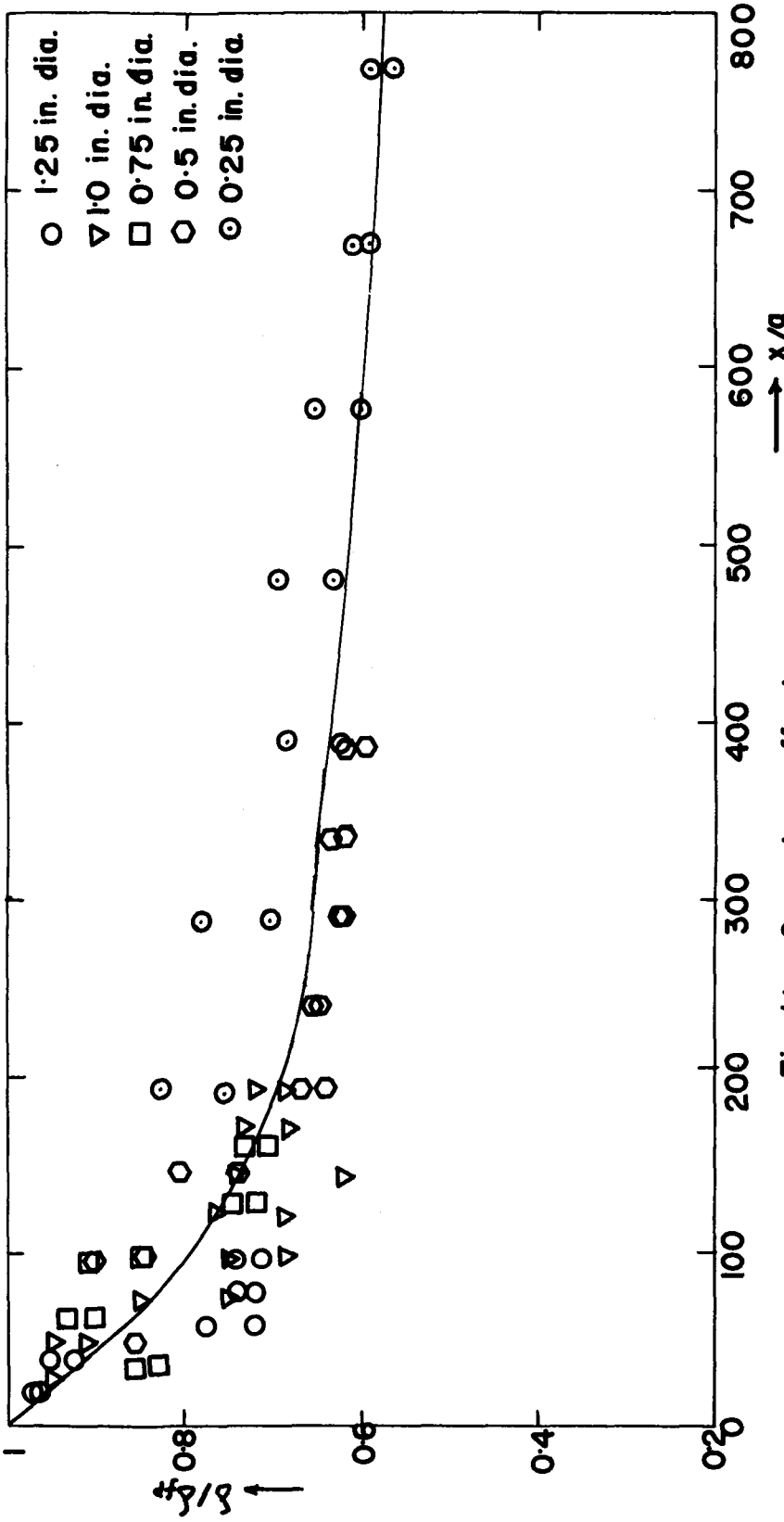

Fig. 11. Curvature effect on boundary layer thickness

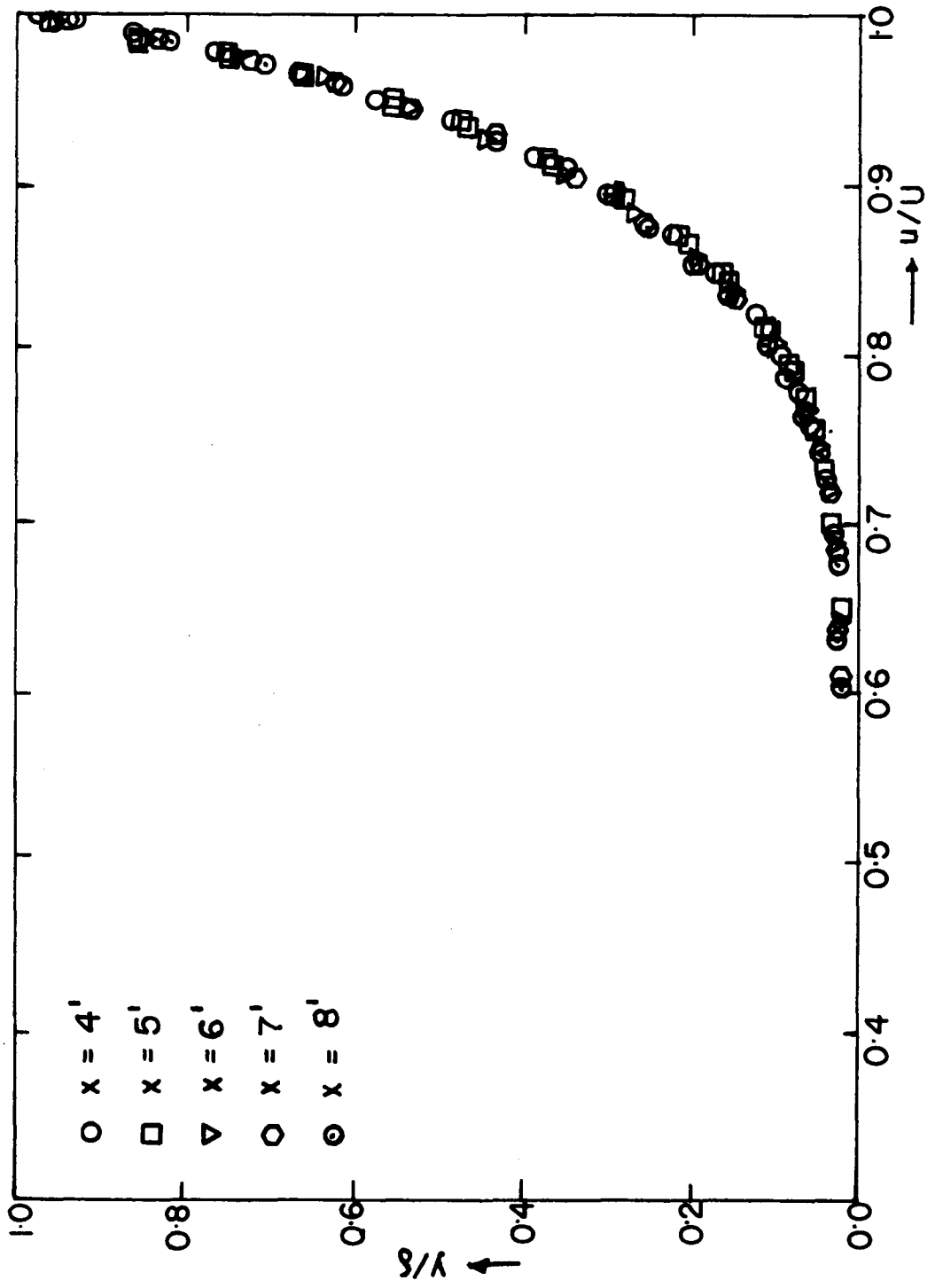

Fig.12. Nondimensional velocity profiles of 0·5 in. dia. cylinder

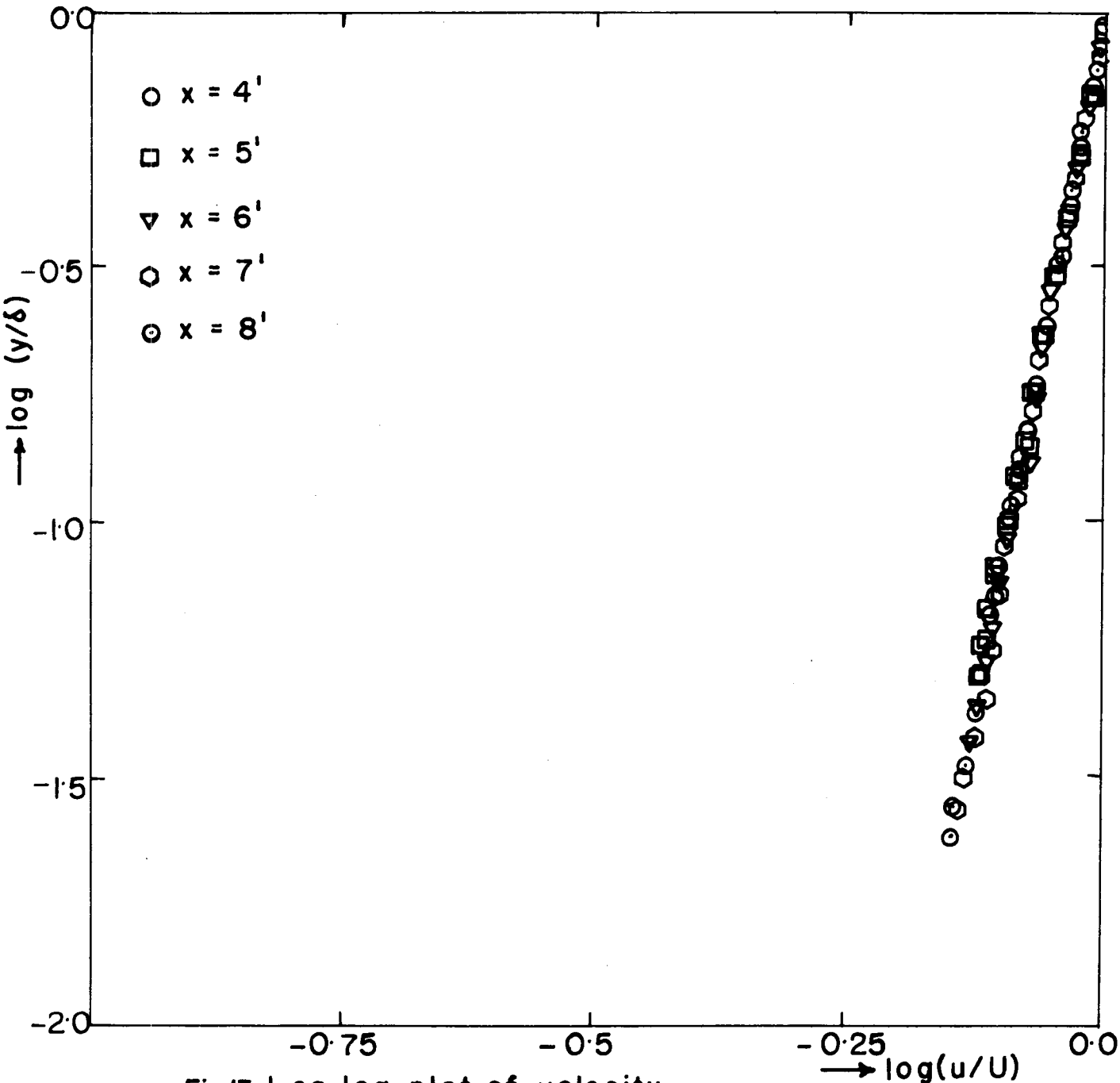

Fig.13. Log log plot of velocity profiles of 0·5 in. dia. cylinder.

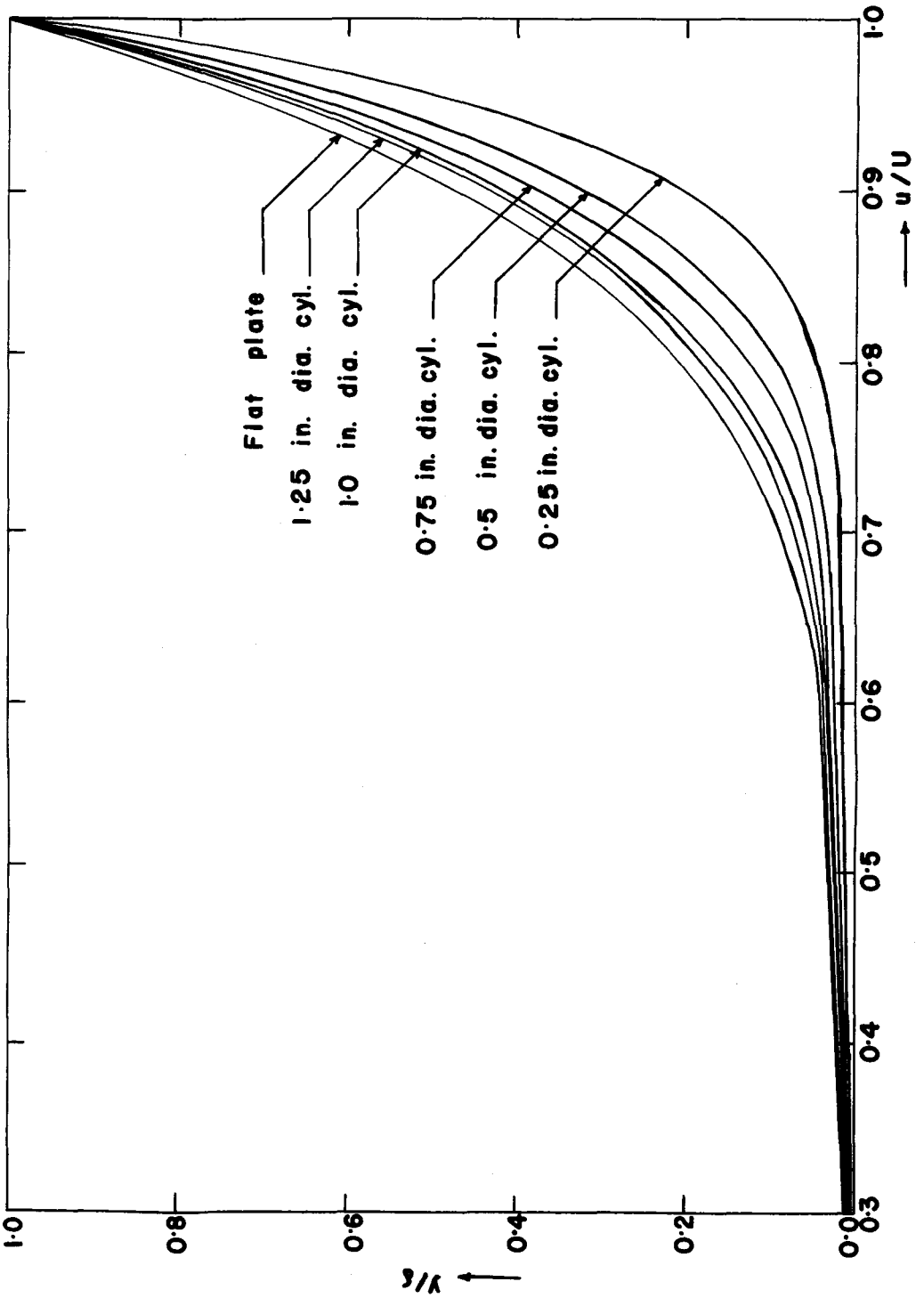

Fig.14. Nondimentional velocity profiles

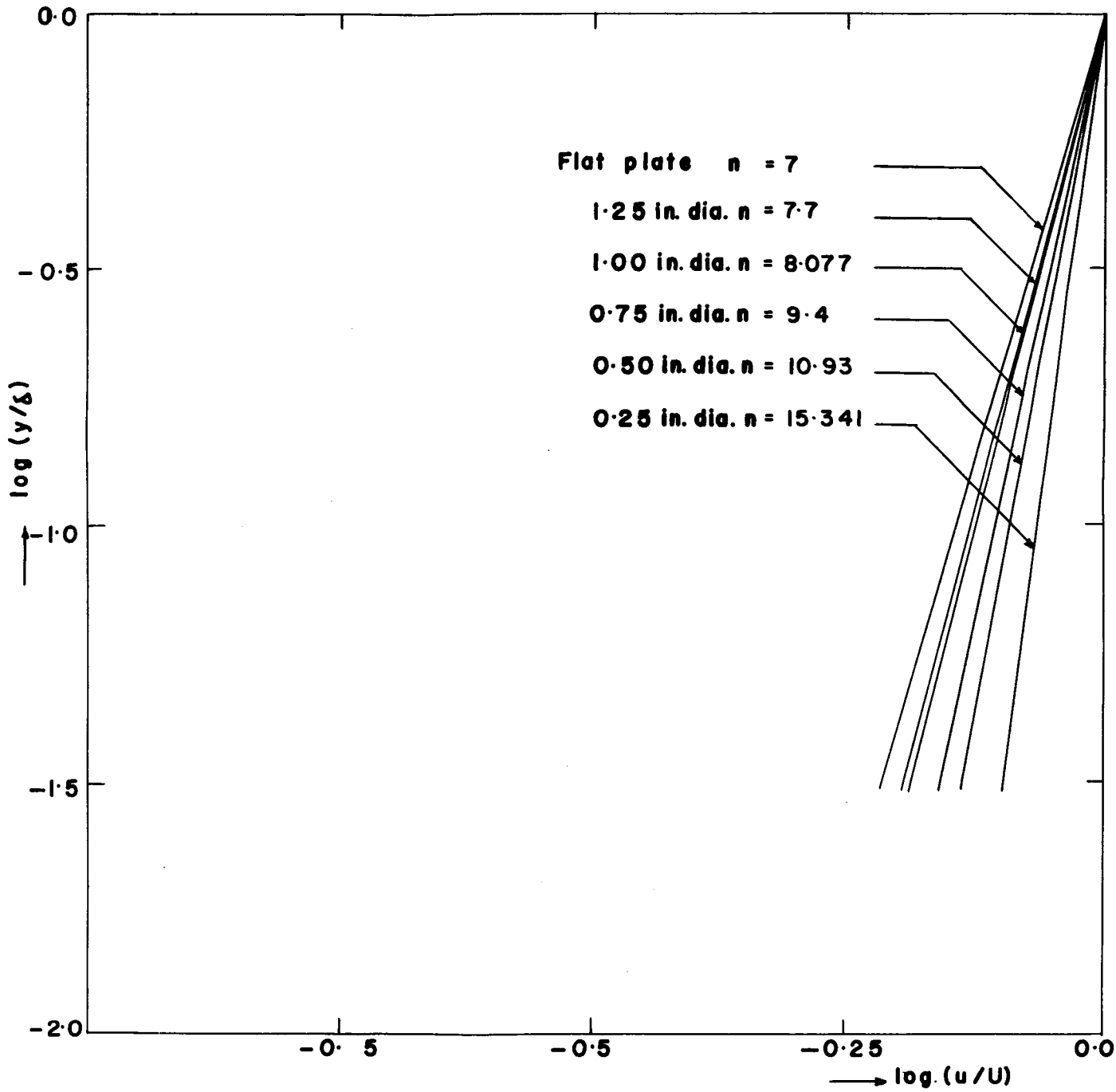

Fig.15. n for different cylinders

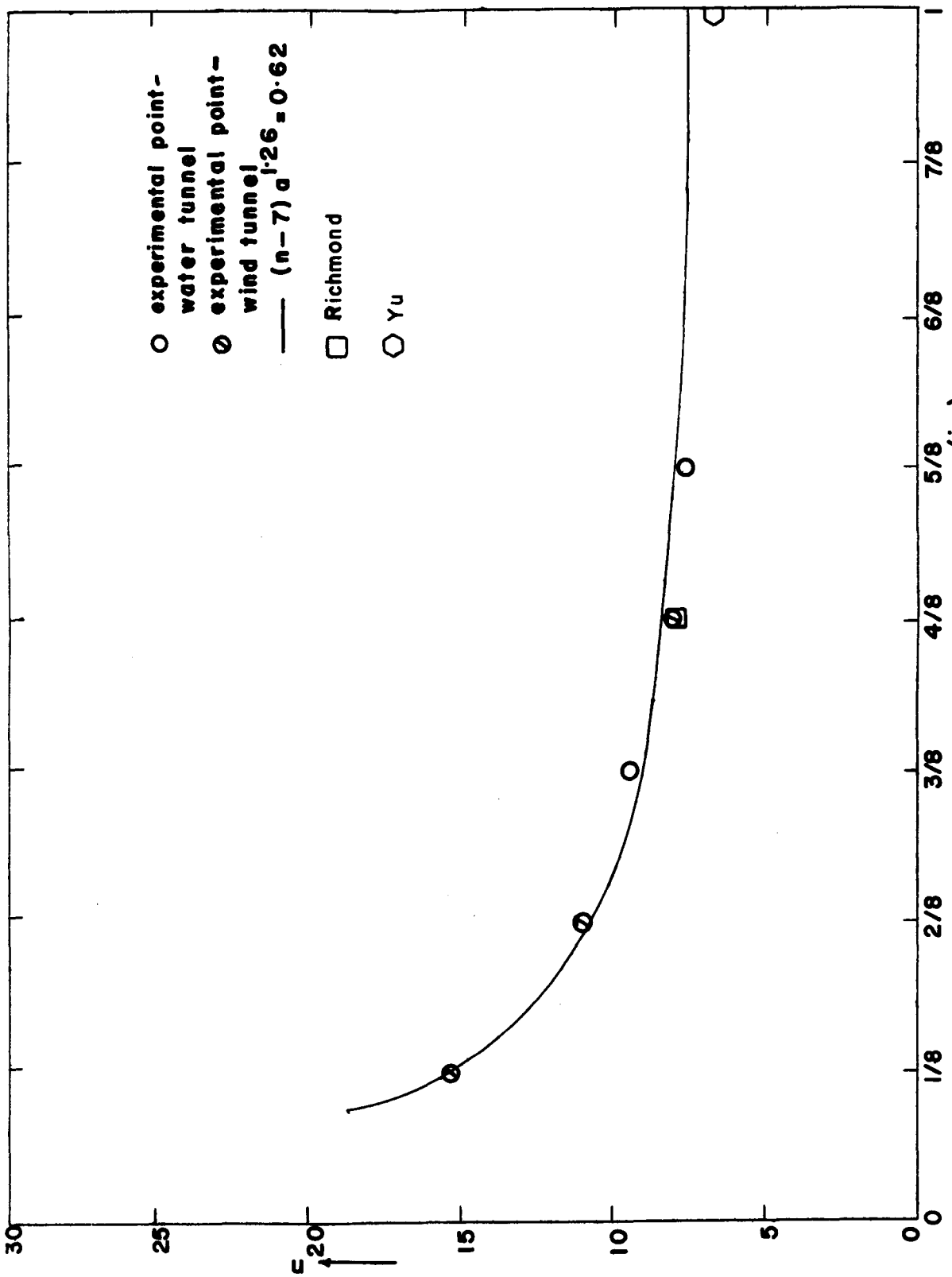

Fig.16. Relation of n to cylinder radius

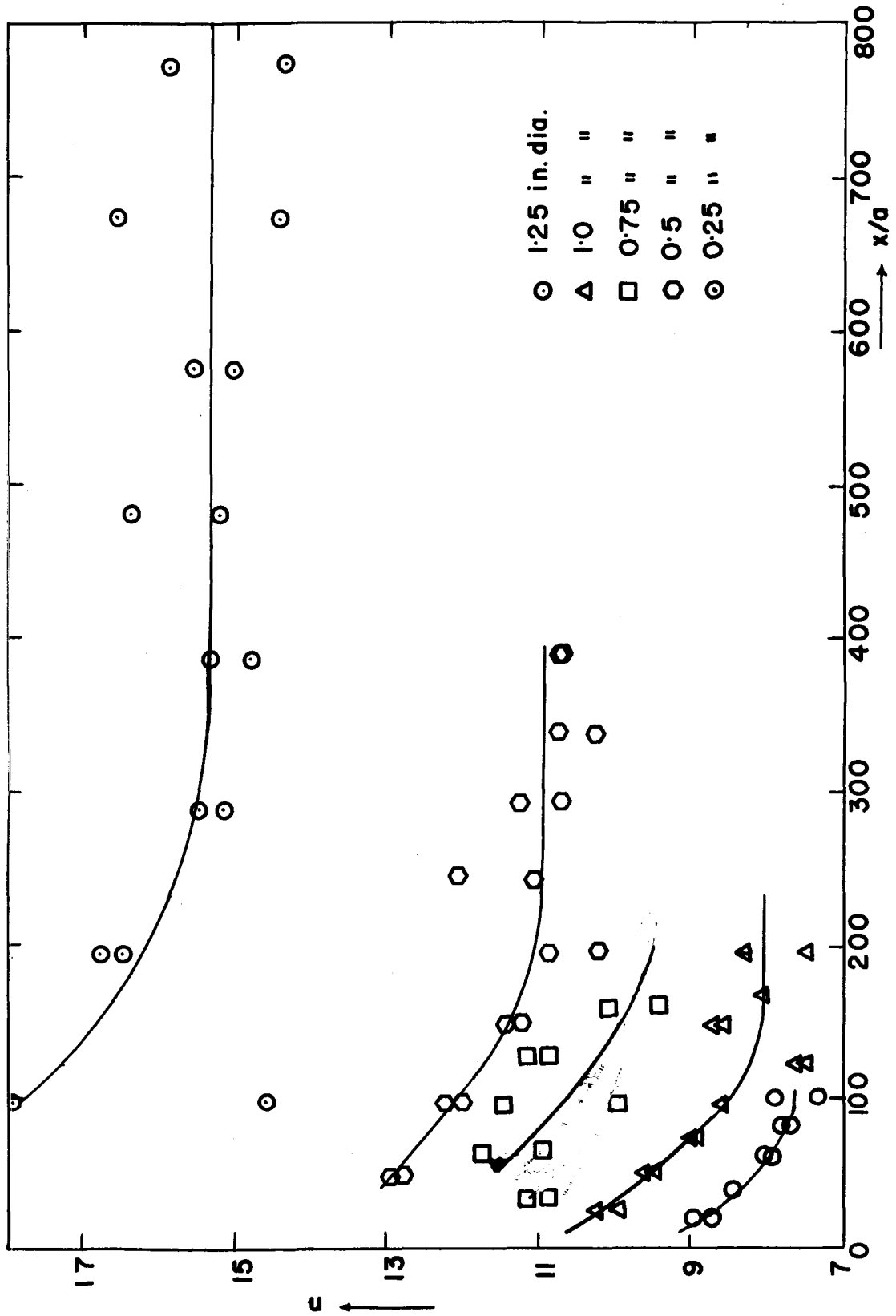

Fig. 17. n vs. axial distance

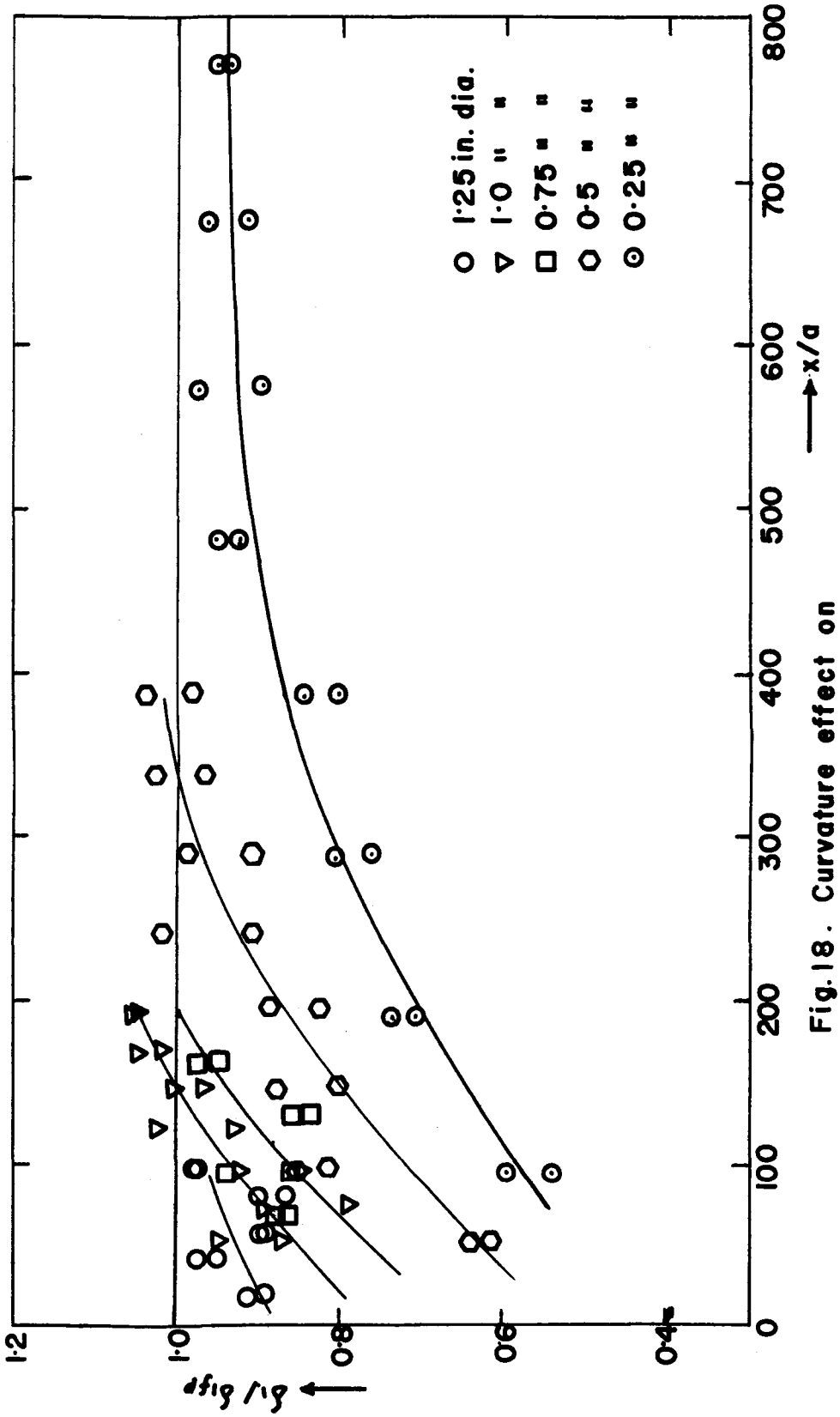

Fig. 18. Curvature effect on displacement thickness

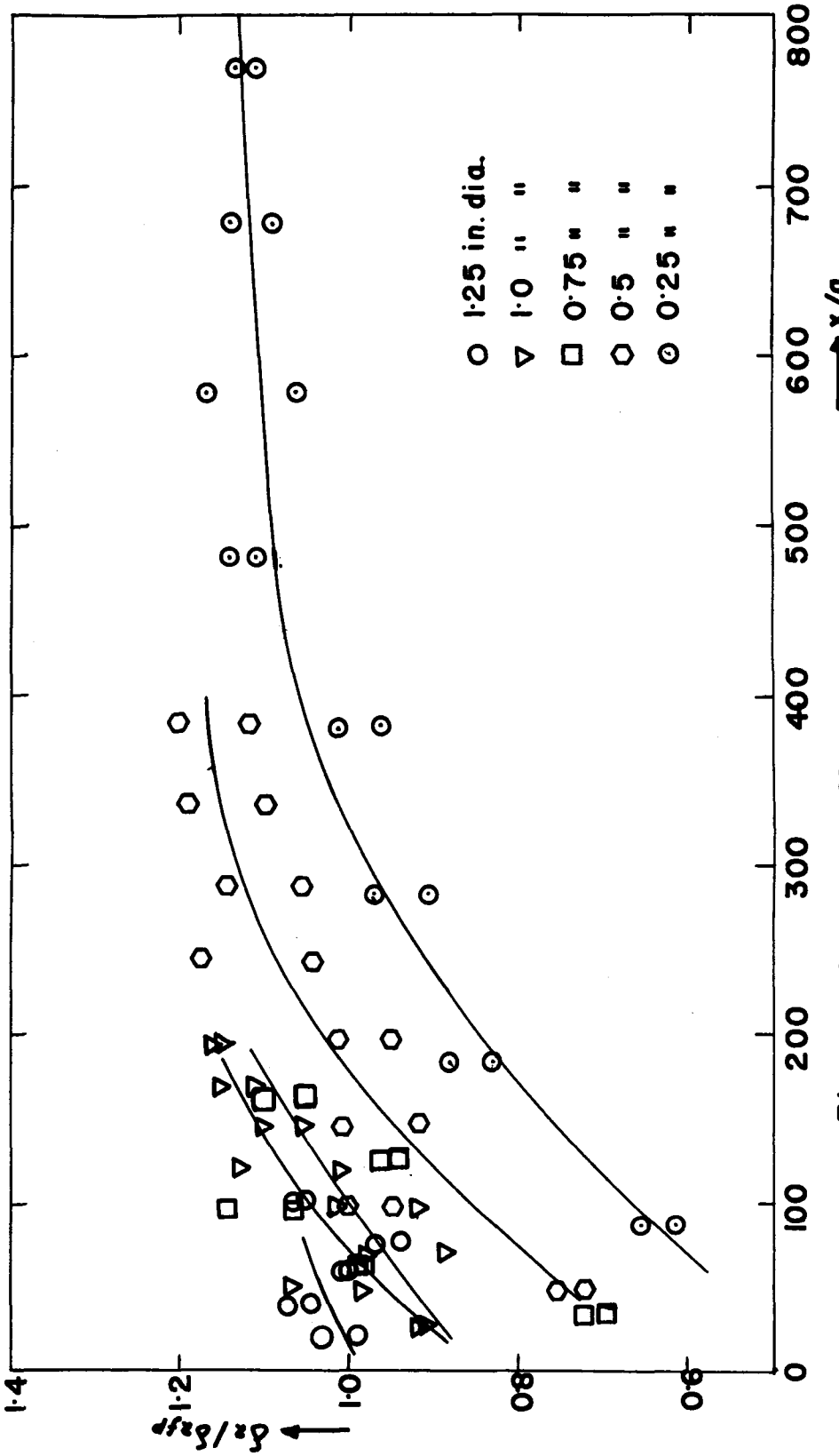

Fig.19. Curvature effect on momentum thikness

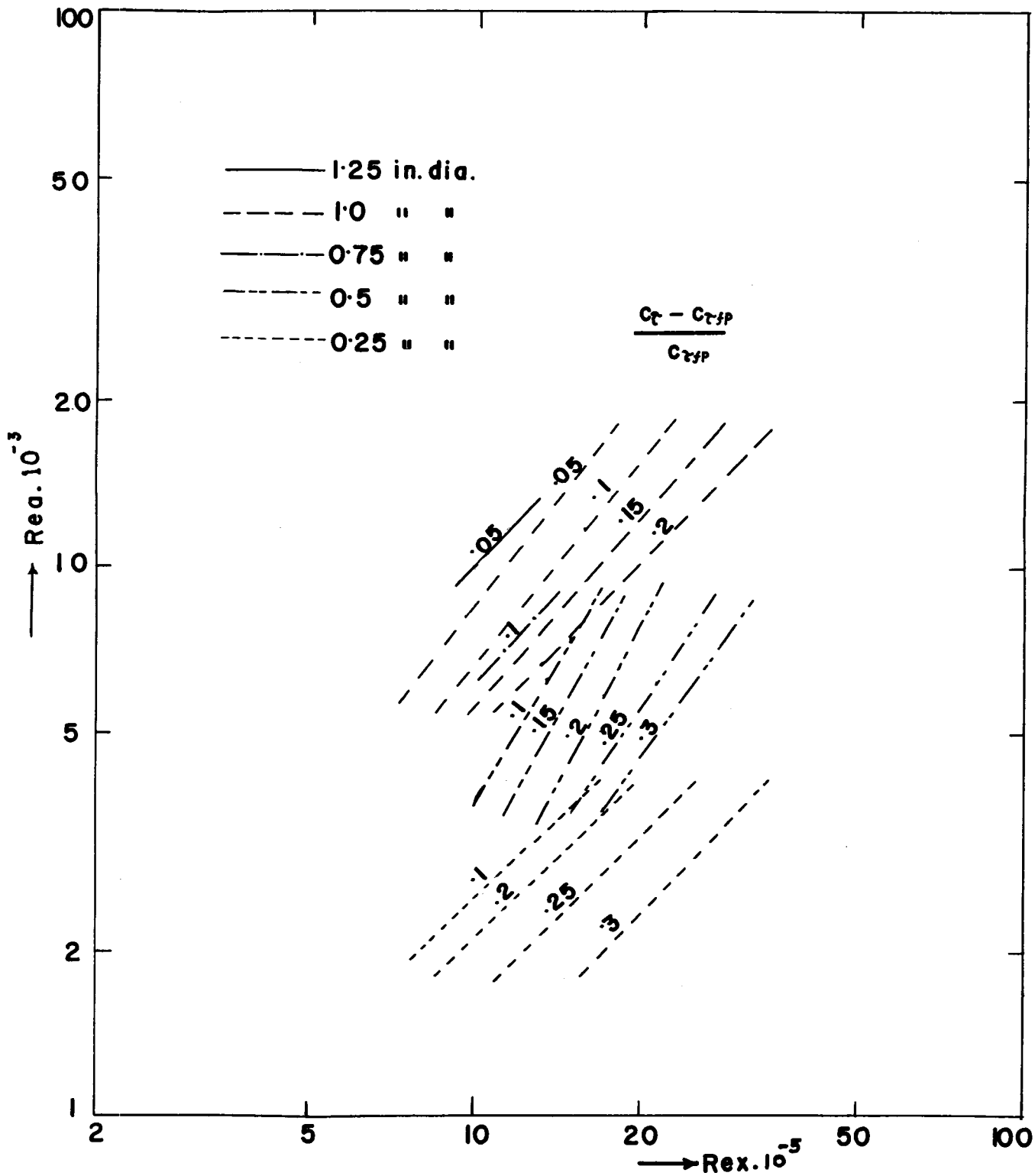

Fig. 20 Local friction coefficient.

APPENDIX 1

Computer programme:

$$(n-7) = \frac{k_2}{a^{k_1}}$$

The numerical values of k_1 and k_2 were determined by solving the above equation parametrically, adopting the method of least squares. The computational strategy was as follows:

For each value of a, n was calculated using the starting values of parameters k_1 and k_2. The sum of squares of residuals (nobs - ncalc) was determined and the function F was calculated using the following relation:

$$F = 100 \sqrt{\frac{(nobs - ncalc)^2}{M - 1}}$$

where M is the number of data points.

The object of the programme is to fix the numerical values of k_1 and k_2 so as to minimize the function F.

The subroutine FUNMIN alters the parameters k_1 and k_2 and calls the subroutine FUNVAL to calculate the new value of F_1 with the new values of k_1 and k_2 and returns the control to FUNMIN. F_1 is compared with F_o and the parameters readjusted so as to push the function F towards the minimum. This process is repeated until at any stage, for each parameter, the ratio

$$\left(\frac{\text{current value of the parameter}}{\text{previous value of the parameter}} - 1\right)$$

becomes less than E where E is a variable fixed in the

present case as 10^{-6}. The subroutine FINFUN calculates n for each value of a using the final values of k_1 and k_2 as the best values.

APPENDIX I

A Programme for Linear Least Squares Fit for the Correlation of n and Radii of Cylinders, written in FORTRAN IV Language

MAIN

```
      COMMON M, R(50), P(50)
      DIMENSION X(16), IRUN(18)
      READ(5,111) M, (R(I), P(I), I=1,M)
111   FORMAT (I3/(2F10.0))
112   READ (5,113) IRUN
113   FORMAT(1H1, 2X, 18A4)
      WRITE (6, 113) IRUN
114   READ (5,115) L
115   FORMAT (I3)
116   READ (5,117) N,E,IPRINT, (X(I), I= 1,N)
117   FORMAT (I2/F10.0/I2/(2F6.3))
      WRITE (6,118) E, (X(I), I=1,N)
118   FORMAT (9H0 ERROR =,F10.6, 3X,34H STARTING VALUES OF PAR-
                  AMETERS ARE,
     116(3X,F10.3))
      RES=0.
      L=L-1
      CALL FUNMIN (N,L,X, RES,E,IPRINT)
      WRITE (6,119) RES, (X(I), I= 1,N)
119   FORMAT (1H0, 2X,E11.4, 16(2X,F7.4))
      STOP
      END
```

```
      SUBROUTINE FUNMIN (N,L,X,RES,E,IPRINT)
      DIMENSION X(16), F(16), P(16),XX(16),HH(16),Z(16,16)
      EQUIVALENCE (FF,F2),(A,F3,H),(B,YW)
      DO 2 I=1,N
      DO 3 J=1,N
    3 Z(I,J)=0.
      HH(I) =0.5*X(I)
    2 Z(I,I)=1.
      CALL FUNVAL (L,X,F1)
    6 DO 4 I=1,N
    4 P(I) = X(I)
      Y0 = F1
      DO 777 I=1,N
      LINK =0
      GO TO 99
  501 F(I) =FF
  777 Y0 = FF
      DEL = F(1) -F1
      MAX =1
      DO 7 I=2,N
      D=F(I-1) - F(I)
      IF (D-DEL) 7,7,8
    8 DEL =D
      MAX =I
    7 XX(I) = 2.*X(I)-P(I)
      XX(1) = 2.*X(1)-P(1)
      CALL FUNVAL (L,XX,F3)
      IF (F3-F1) 10, 502, 502
   10 IF ((F1-2.*F2+F3)*(F1-F2-DEL)**2-.5*DEL*(F1-F3)**2)11,502,502
   11 IF (MAX-N) 25, 26,25
   25 MAX = MAX+1
      DO 15 I= MAX,N
      DO 14 J= 1,N
   14 Z(I-1,J) = Z(I,J)
   15 HH(I-1) = HH(I)
      A = 0.
   26 DO 16 I=1,N
      B = X(I)-P(I)
      A = ABS(B) + A
   16 Z(N,I) = B
      HH(N) = A
      I = N
      LINK = 2
      GO TO 99
  502 F1 = FF
      IF (IPRINT -1) 19,18,17
   18 WRITE (6,200) FF
      GO TO 19
```

```
 17 WRITE (6,200) L,FF,(X(I), I=1,N)
200 FORMAT (1H0, I3, 2X, E11.4, 16(2X,E11.4))
 19 DO 20 I= 1,N
    IF (ABS(1.-P(I)/X(I)) -E) 20, 6, 6
 20 CONTINUE
    RES = FF
    CALL FINFUN (X)
    RETURN
 99 H = .2*HH(I)
    LINK2 = 1
    GO TO 100
111 CALL FUNVAL (L,X,Y1)
    IF (Y1-Y0) 85, 85, 83
 83 H = -H
    LINK2 = 2
    GO TO 100
112 YW = Y0
    Y0 = Y1
    Y1 = YW
    GO TO 85
 80 Y0 =Y1
    Y1 = Y2
 85 H = H+H
    LINK2 = 3
    GO TO 100
113 CALL FUNVAL (L,X,Y2)
    IF (Y2 -Y1) 80, 80, 90
 90 HH(I) = H
    H = H*(.75*(Y1-Y2)/(Y2-3.*Y1+Y0+Y0) -.5)
    LINK2 =4
100 DO 101 J= 1,N
101 X(J) = H*Z(I,J) + X(J)
    GO TO (111,112,113,114), LINK2
114 CALL FUNVAL (L,X,FF)
    IF (LINK) 502, 501, 502
    END
```

FUNVAL

```
      SUBROUTINE FUNVAL (L,X,F1)
      COMMON M,R(50), P(50)
      DIMENSION X(16), PCALC(50)
      SUM = 0.
      DO 999 J = 1,M
      PCALC(J) = (X(2)/(R(J)**X(1))) + 7.0
  999 SUM = SUM + (P(J) - PCALC(J))**2
      F1 = 100.*SQRT(SUM/FLOAT(M-1))
      WRITE (6, 998) L,F1
  998 FORMAT (24H0 NUMBER OF ITERATION = ,I5, 3X,
                          11HFUNCTION = ,E11.4)
      L = L+1
      RETURN
      END
```

FINFUN

```
      SUBROUTINE FINFUN (X)
      COMMON M, R(50), P(50)
      DIMENSION X(16), PCALC(50), DIFF(50)
      DO 998 J = 1,M
      PCALC(J) = (X(2)/(R(J)**X(1))) +7.0
  998 DIFF(J)  = P(J) -PCALC(J)
      WRITE (6,997) M
  997 FORMAT (1H0,10X, 36H RAD(IN)   IND(OB)  IND(CA)     DIFF,
                              5X, 2HM=, I3,//)
      WRITE (6,996) (R(J), P(J), PCALC(J), DIFF(J), J=1,M)
  996 FORMAT (13x, F5.3, 4X, F6.3, 3X, F6.3, 5X, F6.3)
      RETURN
      END
```

APPENDIX. 2.

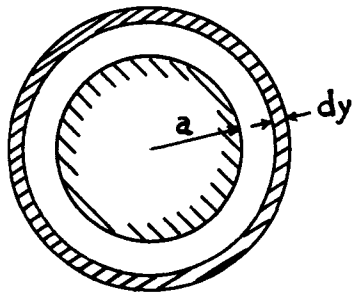

Consider an elemental ring of width dy concentric with the cylinder.

Let the radius of the ring be = a+y

The area of the ring is $2\pi(a+y)\,dy$

Let the velocity in this area be = u

Then

$$U\,2\pi\,\delta_1\,a = \int_0^{\delta} (U-u)\,2\pi\,(a+y)\,dy$$

$$\delta_1 = \int_0^{\delta} (1-u/U)\,(1+y/a)\,dy$$

APPENDIX. 3.

$$u/U = (y/\delta)^{1/n} \qquad 1$$

$$u_\tau = (\tau a/\rho)^{1/2} \qquad 2$$

from eqns. 1 and 2

$$u/u = C \left(\frac{y u_\tau}{\nu}\right)^{1/n} \qquad 3$$

$$\tau a = \rho\, C^{-2n/(1+n)}\, U^{2n/(1+n)} \left(\frac{\nu}{\delta}\right)^{2/(1+n)} \qquad 4$$

$$\delta_2 = \int_0^\delta u/U\,(1-u/U)\,(1+y/a)\,dy \qquad 5$$

$$\frac{\tau a}{\rho U^2} = \frac{c_f}{2} = \frac{d\,\delta_2}{dx} \qquad 6$$

from eqns. 5 and 6

$$\tau a = \rho U^2 \frac{d}{dx} \int_0^\delta u/U\,(1-u/U)\,(1+y/a)\,dy$$

$$= \rho U^2 \frac{d}{dx} \int_0^\delta (y/\delta)^{1/n} (1-y/\delta)^{1/n} (1+y/a)\,dy$$

$$= \rho U^2 \frac{d}{dx} \frac{1}{\delta^{1/n}} \int_0^\delta (y^{1/n} - y^{2/n}/\delta^{1/n})\,dy$$

$$+ \frac{\rho U^2}{a} \frac{d}{dx}\, 1/\delta^{1/n} \int_0^\delta y^{1/n} \left[1-(y/\delta)^{1/n}\right] y\,dy$$

$$= \rho U^2 \frac{d}{dx} \left[\frac{\delta^{1+1/n}}{\delta^{1/n}(1+1/n)} - \frac{\delta^{1+2/n}}{(1+2/n)\,\delta^{2/n}}\right]$$

$$+ \frac{\rho U^2}{a} \frac{d}{dx} \left[\frac{\delta^{2+1/n}}{\delta^{1/n}(2+1/n)} - \frac{\delta^{2+2/n}}{\delta^{2/n}(2+2/n)}\right]$$

$$\tau_a = \rho U^2 \frac{d}{dx}\left[\frac{n\delta}{1+n} - \frac{n\delta}{2+n}\right] + \frac{\rho U^2}{a}\frac{d}{dx}\left[\frac{\delta^2 n}{1+2n} - \frac{\delta^2 n}{2+2n}\right]$$

$$= \rho U^2 \left(\frac{(n+2)-(n+1))n}{(1+n)(2+n)}\right)\frac{d\delta}{dx} + \frac{\rho U^2}{a}\frac{n}{(1+2n)(2+2n)}\frac{d\delta^2}{dx}$$

$$= \rho U^2 \left[\frac{n}{(n+1)(n+2)} + \frac{n}{(2n+1)(n+1)}\frac{\delta}{a}\right]\frac{d\delta}{dx} \qquad 8$$

combining with equation 6

$$\left[\frac{n}{(n+1)(n+2)} + \frac{n}{(2n+1)(n+1)}\frac{\delta}{a}\right]\frac{d\delta}{dx} = C^{-2n/(1+n)}\, U^{2n/(1+n)-2}\, (\nu/\delta)^{2/(1+n)}$$

$$\left[\frac{n}{(n+1)(n+2)}\delta^{2/(1+n)} + \frac{n}{(2n+1)(n+1)}\frac{\delta^{(3+n)/(1+n)}}{a}\right]\frac{d\delta}{dx} =$$

$$C^{-2n/(1+n)}\, U^{-2/(1+n)}\, \nu^{2/(1+n)}$$

integrating

$$\frac{n}{(n+1)(n+2)}\frac{(1+n)}{(3+n)}\delta^{(3+n)/(1+n)} + \frac{n(1+n)}{(2n+1)(n+1)(4+2n)}\frac{\delta^{(4+2n)/(1+n)}}{a}$$

$$= C^{-2n/(1+n)}\, U^{-2n/(1+n)}\, \nu^{2/(1+n)}\, x$$

$$\frac{n}{(n+2)(n+3)}\delta^{(3+n)/(1+n)} + \frac{n\delta}{(2n+1)(n+2)}\frac{\delta^{(3+n)/(1+n)}}{2a} = C^{-2n/(1+n)}$$

$$U^{-2/(1+n)}\, \nu^{2/(1+n)}\, x$$

$$\frac{n}{(n+2)(n+3)}\,\delta^{(3+n)/(1+n)}\left[1+\frac{(n+3)}{(2n+1)2}\,\frac{\delta}{a}\right] = C^{-2n/(1+n)}$$

$$U^{-2/(1+n)}\,\gamma^{2/(1+n)}\,x$$

$$\delta\left[1+\frac{n+3}{2\,(2n+1)}\,\frac{\delta}{a}\right] = \left[\frac{n}{(n+2)(n+3)}\right]^{-(1+n)/(3+n)}$$

$$C^{-2n/(n+3)}\,x\,Rx^{-2/(n+3)} \qquad 9$$

REFERENCES

1. Burgers, J. M., The Motion of a Fluid in the Boundary Layer Along a Plane Smooth Surface. Proc. First Int. Congress for Appl. Mech. 113, Delft 1924.

2. Zijnen, B.G.H., Measurement of the Velocity Distribution in the Boundary Layer Along a Plane Surface. Thesis, Delft 1924.

3. Kempf, G., Flachenwiderstand, Werft-Reederei-Hafen, pp 521-528, 1924.

4. Karhan, K., Der Einflus von Sandrauhigeit auf den Reibungswiderstand Schiff-und-Hafen, pp 8-10, 1952.

5. Hughes, G., Friction and Form Resistance in Turbulent Flow, and a Proposed Formulation for Use in Model and Ship Correlation. TINA vol.96, 1954.

6. Richmond, R.L., Experimental Investigation of Thick, Axially Symmetric Boundary Layers on Cylinders at Subsonic and Hypersonic Speeds. GALCIT Hypersonic Research Project Memo No. 39, 1957.

7. Yu, Y.S., Effects of Transverse Curvature on Turbulent Boundary Layer Characteristics. J. Ship Research, vol.2, pp 33-51, Dec. 1958.

8. Yasuhara, M., Experiments on Axisymmetric Boundary Layers Along a Long Cylinder in Incompressible Flow. Trans. Japan Soc. Aero Space Sci. vol. 2, No.3, pp 72-76, 1959.

9. Bonsignore, A., Transverse Curvature Effect. A Dissertation Submitted to the Faculty of Applied Science, University of Windsor, 1966.

10. Singh, P.P., The Submerged Cylindrical Surface Jet. Ph.D. Thesis, University of Saskatchewan, May, 1966.

11. Shirtliffe, G.J., Effect of Transverse Curvature on Low Speed Turbulent Boundary Layer Flow Along Circular Cylinders. M.Sc. Thesis, University of Minnesotta, 1962.

12. Venkatasubramanian, R., Effect of Transverse Curvature on Turbulent Fluid Flow and Heat Transfer Characteristics. Ph.D. Thesis, University of Saskatchewan, 1968.

13. Landweber, L. Effect of Transverse Curvature on Frictional Resistance. David W. Taylor Model Basin, U.S. Navy Report 689, 1949.

14. Eckert, H.U., Simplified Treatment of the Turbulent Boundary Layer Along a Cylinder in Compressible Flow. J. Aero Sci. vol. 19, pp23-29, 1958.

15. Karhan, K., The Axial Frictional Resistance of Long Cylinders in Turbulent Flow. J. Ship Research vol. 3, pp 24-28, Oct. 1959.

16. Telfer, E.V., Frictional Resistance and Ship Similarity. TINA vol. 92, 1950.

17. Ginevskii, A.S., Solodkin, E.E., The Effect of Lateral Surface Curvature on the Characteristics of Axially Symmetric Turbulent Boundary Layers. J. App.Math. and Mech., vol. 22, pp 1169-1179, 1958.

18. Sasajima, H., Takaji, M., Tanaka, I., Theoretical Research on Frictional Resistance of a Flat Plate of Finite Breadth and a Circular Cylinder in Axial Motion. Technology Report of the Osaka University, vol. 9, No. 345, pp 67-77, March 1957.

19. Reid, R.O., Wilson, B.W., Boundary Flow Along a Circular Cylinder. Proc. ASCE, J.Hydr. Div., vol. 3, pp 21-40, May 1963.

20. Sparrow, E.M., Eckert, E.R.G., Minkowycz, W.J., — Heat Transfer and Skin Friction for Turbulent Boundary Layer Flow Longitudinal to a Circular Cylinder. Trans. ASME, J.App. Mech., vol. 30, pp 37-43, March 1963.

21. Rao, G.N.V., — The Law of the Wall in a Thick Axisymmetric Turbulent Boundary Layer. J. App. Mech., Trans. ASME. Series E 34, pp 237-238, March 1967.

22. Landweber, L., Siao, T.T., — Comparison of Two Analyses of Boundary Layer Data on a Flat Plate. J. Ship Research, March 1958.

23. Preston, J.H., — The Determination of Turbulent Skin Friction by Means of Pitot Tubes. J. Royal Aeronautical Soc. vol. 58, Feb. 1954.

24. Nikuradse, J. — See "Boundary Layer Theory" by Schlichting, H., Edition 4, Pg. 505.

VITA AUCTORIS

1943 Born in India on February 12.

1959 Completed high school at Gov't High School Muvattupuzha, Kerala, India in April.

1966 Received the degree of Bachelor of Engineering in Mechanical Engineering, from the University of Mysore, Mysore, India.

1969 Currently a candidate for the Degree of Master of Applied Science in Mechanical Engineering at the University of Windsor.